RELATIVE PERMEABILITY ANALYSES TO DESCRIBE MULTI-PHASE FLOW IN CO_2 STORAGE RESERVOIRS

SALLY BENSON, RONNY PINI

STANFORD UNIVERSITY, DEPARTMENT OF ENERGY RESOURCES ENGINEERING, STANFORD, USA

CATRIONA REYNOLDS, SAMUEL KREVOR

IMPERIAL COLLEGE LONDON, DEPARTMENT OF EARTH SCIENCE AND ENGINEERING, LONDON, UK

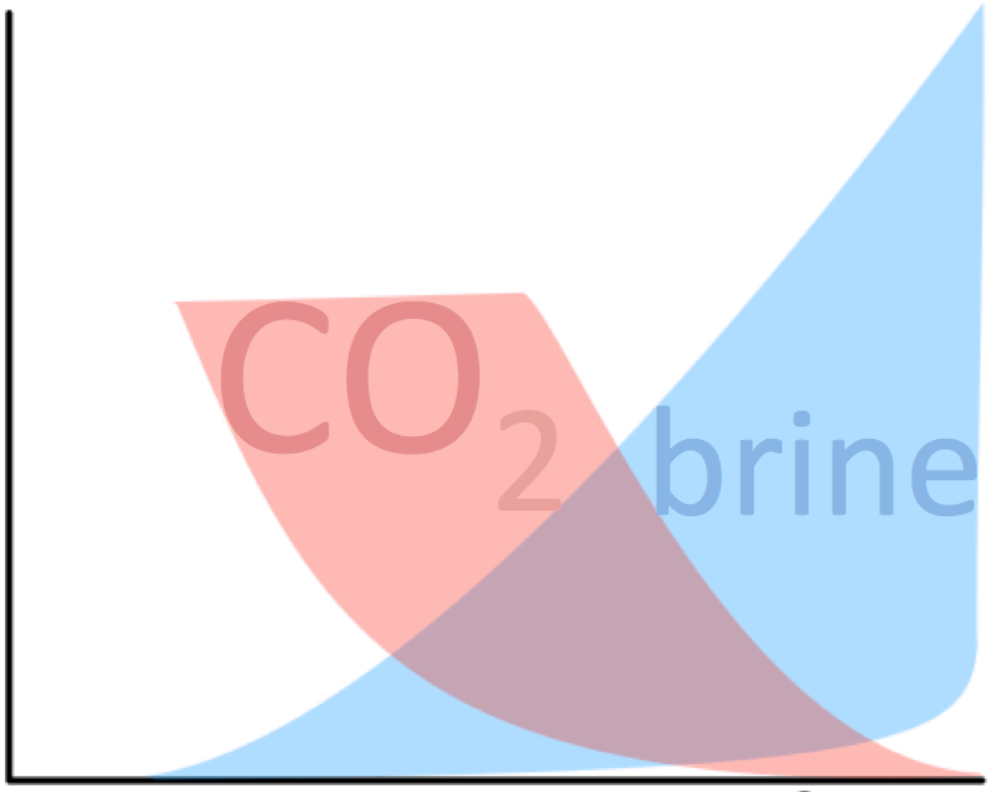

SUPPORTED BY

GLOBAL CCS INSTITUTE

1. Introduction

Relative permeability is one of the most important properties influencing the fate and transport of CO_2 in the subsurface. It is a parameter that quantifies the extent to which the injected CO_2 and water interfere with each other as they migrate through rocks. To one degree or another it affects almost all of the important aspects of a storage project: the spatial extent of the CO_2 plume, the injectivity of a well, extent of capillary trapping, and leakage through the seal are all influenced by relative permeability. Relative permeability measurements are also used directly in all of the mathematical approaches for predicting and matching the fate and transport of CO_2 in the subsurface. Consequently, accurate measurements for this important parameter are indispensable.

The concept of relative permeability was established nearly a century ago, finding application in agriculture, as well as, oil and gas recovery. Beginning in the 1960s, a new wave of interest grew through the fields of contaminant hydrology and nuclear waste storage. In the late 1990s, as CO_2 storage emerged as an important option for reducing greenhouse gas emissions, once again, the need for new understanding arose. One might reasonably ask why a concept established nearly a century ago would remain a topic of discussion.

The origin of the ongoing discussion stems from the fact that, in practice, relative permeability is an empirical parameter that depends on the specific context in which it is being applied. For example, in oil recovery, one of the primary interests in relative permeability grew out of the water-flooding of depleted oil fields. Water was injected into a reservoir to displace and increase oil recovery. In this case water, the so-called wetting fluid was used to displace oil the non-wetting fluid, oil. Scientifically, this is referred to as an imbibition process. Consequently, it was necessary to measure relative permeability during imbibition. On the other hand, for CO_2 storage in a saline formation, CO_2, the non-wetting fluid, is injected into a brine-filled reservoir. This is called a drainage process and relative permeability under these conditions is required. Relative permeability can also depend on the heterogeneity of the rock, the spatial scale of the measurements, and arguably, on the method for making the measurement. As a result of these and other factors, relative permeability remains a topic of relevance and continued interest.

The purpose of this report is to provide an explanation of the different methods used to measure relative permeability, an objective review of comparable methodologies, and discuss aspects of drainage vs. imbibition analyses. The report will also address issues such as the influence of rock heterogeneity and boundary conditions on the measured relative permeability curves. The scope will also include the identification of data gaps and the requirements to obtain additional material to provide a relatively complete library of relative permeability measurements in varying brine compositions and rock types to represent as complete a suite of potential storage sites as possible.

2. Background on Multiphase Flow Properties

The conceptual framework for multiphase flow in porous media is briefly reviewed in this section. For further detail and the history of the development of these concepts, the readers are referred to seminal references on the subject, including those by *Bear* [1], *Dullien* [2], *Lake* [3].

2.1. **Continuum rock properties.**

The continuum description of the properties of a porous media through which fluid is flowing includes the porosity, ϕ [-] and permeability, k [m^2]. The porosity is the fraction of the bulk volume of the medium which is available for fluid flow, e.g. if the void volume is denoted by V_v and the solid volume denoted by V_s,

$$\phi \equiv \frac{V_\mathrm{v}}{V_\mathrm{T}} = \frac{V_\mathrm{v}}{V_\mathrm{v} + V_\mathrm{s}}. \tag{1}$$

The permeability, or intrinsic permeability, is defined by the general form of Darcy's law [5]

$$q = -\frac{k}{\mu}\nabla\Phi, \tag{2}$$

where q [m/s] is a velocity known as the Darcy velocity[1], μ [Pa·s] is the dynamic viscosity of the fluid, ∇ is the Nabla operator and $\Phi \equiv P + \rho g z$ represents the fluid potential with components of pressure and gravitational potential, where P [Pa] is the fluid pressure, ρ [kg/m^3] is the fluid density, $g \approx 9.8$ m/s^2 is acceleration due to gravity, and z [m] is a spatial coordinate in the vertical direction (i.e. with or opposite to the direction of the gravitational force).

In a multiphase flow system consisting of N_p phases, the saturation, S_α [-], is defined as the fraction of the pore space filled by fluid α,

$$S_\alpha \equiv \frac{V_\alpha}{\sum_i V_i} \qquad i = 1, ..., N_\mathrm{p} \tag{3}$$

where i denotes the phase index and therefore $\sum_i V_i = V_\mathrm{v}$, thus implying that $\sum_i S_i = 1$.

2.2. **Multiphase Flow Properties.**

[1]The average fluid velocity, v, is given by the Darcy velocity divided by the porosity, $v = q/\phi$.

2.2.1. *Interfacial Properties And The Concept of Wetting.* Geologic formations are often referred to as capillary systems, as the mechanical equilibrium between the resident fluids in their porous structure is governed not only by hydrostatic and gravity forces, but also by capillary action [2]. The latter is the result of the interfacial forces acting between fluid phases as well as between fluid and solid phases, and gives rise to the unique nature of multiphase flow through porous media. Due to the configuration of molecules at the interfaces of two phases, the interface has an associated energy per unit surface area. This energy is usually described as a force per unit distance, and the interfacial tension γ_{ij} [mN/m] is used to describe the energy inherent in the interface between two phases i and j. This energy is responsible for the pressure difference that exists across an interface separating two immiscible fluids, i.e. the capillary pressure.

For fluid-solid interfaces, the contact angle θ at the fluid-fluid-solid interface is used to characterize the balance of interfacial forces between fluid-fluid and fluid-solid interfaces through the Young-Laplace equation,

$$\cos\theta = \frac{\gamma_{\mathrm{w,s}} - \gamma_{\mathrm{nw,s}}}{\gamma_{\mathrm{w,nw}}}, \tag{4}$$

where the subscripts s refers to the solid phase, while the subscripts w and nw denote fluid phases as *wetting* and *nonwetting*, respectively. The angle is measured in the wetting phase, which has a stronger affinity for the mineral surface than the nonwetting phase. For rocks in their natural state (i.e. unaltered by organic materials), water is the wetting phase and liquids made of non-polar molecules the nonwetting phase.

2.2.2. *The Relative Permeability Curve.* The definition of relative permeability arises from the description of the concurrent flow of multiple fluids through a porous media using Darcy's law. The presence of a second fluid phase increases the resitance to flow for the other fluid. It is generally observed that the permeability to each fluid phase, and the sum of permeability to both phases, will be less than that of the intrinsic permeability of the rock. Applying Darcy's law to each fluid phase, i,

$$q_i = -\frac{k_i}{\mu_i}\nabla\Phi_i \qquad i = 1, ..., N_{\mathrm{p}}. \tag{5}$$

Here k_i is the *effective permeability* of phase i and N_{p} is the number of immiscible phases. Accordingly, the relative permeability, $k_{\mathrm{r},i}$, of phase i is defined as the ratio of the effective permeability to the intrinsic permeability of the rock,

$$k_{\mathrm{r},i} \equiv \frac{k_i}{k} \qquad i = 1, ..., N_{\mathrm{p}} \tag{6}$$

and Eq.(5) can be rearranged as

$$q_i = -\frac{k_{\mathrm{r},i}k}{\mu_i}\nabla\Phi_i \qquad i = 1, ..., N_{\mathrm{p}} \tag{7}$$

The relative permeability to a fluid phase i is usually assumed to be an increasing function of the saturation of that phase, S_i, so that $k_{\mathrm{r},i} = k_{\mathrm{r},i}(S_i)$. This approach was first developed by

Wyckoff and Botset [6] and *Muskat and Meres* [7] in two coordinated papers. Interestingly, the original experimental work of *Wyckoff and Botset* [6] was performed using CO_2 and brine in large packed sand columns, taking advantage of the solubility of CO_2 in water to create a water-saturated core.

Subsequently, conceptual models have been used to justify the description of multiphase flow with an extended version of Darcy's law, the general suggestions being that the fluid phases flow in separate pore networks with stable interfaces, such that the flow of a given phase resembles that of single phase flow through the pore space albeit with a reduced number of flow pathways [8]. Many observations have shown that this model has little resemblance to the actual processes of multiphase flow at the pore scale, which includes both significant ganglia (or disconnected phase) flow and concurrent flow of wetting and non-wetting phases in single channels (see, e.g., *Avraam and Payatakes* [9], *Kovscek et al.* [10]). Nonetheless, Eq.(7) fulfills the need for a constitutive relationship that can be used in equations of groundwater flow and the Darcy flow model is the nearly exclusively used approach in commercial reservoir simulation today.

Relative permeability curves are traditionally obtained from experimental measurements, as a complete theoretical framework based on accounting for multiphase flow through realistic pore morphologies is still missing [3]. The relative permeability-saturation relationship depends on the rock wettability and on the geometry of the rock's pores [11], the latter effect being particularly evident when comparing unconsolidated vs. consolidated systems [12]. As will be discussed in detail in Section 3, it is not, in general, a strong function of fluid properties [13, 3]. Most importantly, relative permeability is strongly correlated to capillary action: in the absence of capillarity, viscous forces would lead to a uniform distribution of each phase in the pore space of the rock in a proportion corresponding to its saturation, and the relative permeability curves would simplify to two symmetrical diagonal lines intersecting at 50% saturation [2]. This has been shown not to be the case for the vast majority of natural porous systems.

As an example, Figure 1 shows relative permeability data obtained on a Berea Sandstone core using various fluid pairs from the classic dataset of *Oak et al.* [14]. Note that although different fluid pairs are used, the three data sets draw the same two characteristic curves for the nonwetting and wetting phase relative permeability. Additionally, features can be identified from the data that are characteristic of a water-wet system: the relative permeability to the water phase decreases rapidly with increasing nonwetting phase saturation and it vanishes at relatively high water saturations ($\sim$45% in the figure). This observation is usually valid for any system that is strongly wetted by one of the two phases and it is indicative of the nonwetting phases being distributed in the larger (and more conductive) pores [11], thus implying that only a portion of the pore space is substantially contributing to fluid flow. Accordingly, the relative permeability of the nonwetting phase increases with decreasing water saturation and values approaching the intrinsic permeability of the rock are observed at nonwetting saturations much less than 100% [12, 15, 14]. These end-point values represent important landmarks on the relative permeability curves [3]. They are

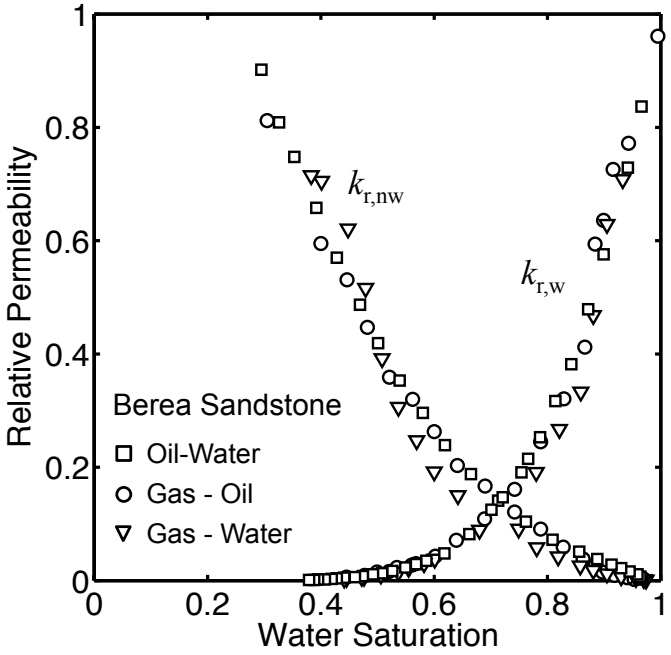

FIGURE 1. Relative permeability curves measured on a Berea Sandstone core with various fluid pairs, namely oil/gas ($\mu_w/\mu_{nw} = 100$ and $\gamma = 25\ mN/m$), water/oil ($\mu_w/\mu_{nw} = 1$ and $\gamma = 50\ mN/m$) and water/gas ($\mu_w/\mu_{nw} = 60$ and $\gamma = 70\ mN/m$). In the study, brine, mineral oil and nitrogen were used as water, oil and gas phases, and the experiments were carried out at pressure of 5.5 MPa and at room temperature [14].

often interpreted to be indicators of the wetting characteristics of the given rock [16] and of certain rock properties that control pore geometry [17].

2.2.3. *Hysteresis in the Relative Permeability Curve.* Relative permeability functions do not depend solely on the saturation, but also on the direction of the saturation change [16]. We refer to *drainage*, when displacement results in a decrease in the wetting phase saturation, and *imbibition* when displacement leads to an increase in wetting phase saturation. Imbibition and drainage curves generally differ from each other. The term hysteresis is used to indicate the irreversibility of multiphase flow. One result of hysteresis is that the non-wetting phase relative permeability during imbibition goes to zero with significant non-wetting phase remaining in the pore space. This is known as *residually trapped* non-wetting phase fluid [4]. A residual nonwetting phase saturation ($S_{nw,r}$) is achieved at the termination of an imbibition curve, and corresponds to the condition of zero capillary pressure (P_c=0). The condition that P_c=0 is not an indication of the absense of capillary

forces, but results from the lack of a connected non-wetting phase across the sample. Additionally, a residual saturation can in principle be referred to as an *irreducible* saturation as it is commonly the case for the wetting phase, although neither irreducible or residual saturations are irreducible in the strict sense of the word [2]. Under the influence of strong viscous forces these residual saturations can be reduced practically to zero due to film instability in the case of the wetting phase [18] and due to the natural repulsion by the rock surface for the nonwetting phase [4].

The impacts of hysteresis are important in situations with strong flow reversals. During cyclic water and gas injection, waterflooding results in the trapping of the gas phase. In the context of CO_2 sequestration, a drainage process takes place at the leading edge of the CO_2 plume, whereby the resident water is displaced by the injected CO_2, and an imbibition process takes place at the trailing edge, where gas is displaced by the return flow of water. This leads to the break-up of the CO_2 phase into bubbles and ganglia, which eventually become immobile [19]. At the macroscopic (continuum) scale, this phenomenon is called residual trapping and its contribution to the immobilization of sequestered CO_2 over the hundred-year time scale can be substantial, as suggested by modeling [20], field test [21] and laboratory data [22, 23]. The trapping characteristics of a given fluid-pair system are commonly presented through the so-called initial-residual (IR) curve, where the maximum (initial) nonwetting phase saturation is plotted as a function of its residual saturation [4] (see Section 6 of this report for examples of IR curves).

2.3. **Standard Correlations for Multiphase Flow Properties.** Several correlations are reported in the literature to describe both the capillary pressure $P_{\mathrm{c}}(S)$ and relative permeability $k_{\mathrm{r}}(S)$ characteristic functions. For the capillary pressure-saturation function the choice of the model is reduced to the Brooks-Corey [15] and the van Genuchten [24] equations, these being the reference cases in the petroleum and hydrology field, respectively. The Brooks-Corey (BC) equation reads as follows,

$$P_{\mathrm{c}} = P_{\mathrm{c,e}} {S^*_{\mathrm{w}}}^{-1/\lambda} \quad \text{or} \quad S^*_{\mathrm{w}} = \left(\frac{P_{\mathrm{c,e}}}{P_{\mathrm{c}}}\right)^{\lambda} \tag{8}$$

where the effective water saturation $S^*_{\mathrm{w}} = (S_{\mathrm{w}} - S_{\mathrm{w,ir}})/(1 - S_{\mathrm{w,ir}})$. The capillary entry pressure, $P_{\mathrm{c,e}}$, the irreducible water saturation, $S_{\mathrm{w,ir}}$, and the so-called pore-size distribution index, λ, are typically used as fitting parameters. Eq. (8) was found to be applicable to a variety of media, including unconsolidated and consolidated systems with a wide range of pore-size distributions (λ=0.5-7.5) [15]. The van Genuchten equation is given by

$$P_{\mathrm{c}} = \frac{1}{\alpha}\left({S^*_{\mathrm{w}}}^{\frac{n}{1-n}} - 1\right)^{\frac{1}{n}} \quad \text{or} \quad S^*_{\mathrm{w}} = \left[(\alpha P_{\mathrm{c}})^n + 1\right]^{\frac{1-n}{n}} \tag{9}$$

where α and n are fitting parameters that are inversely proportional to the nonwetting fluid entry pressure and the width of the pore-size distribution, respectively. It can be easily shown that the VG model approaches asymptotically the BC model as the capillary pressure increases, i.e. as $S^*_{\mathrm{w}} = (\alpha P_{\mathrm{c}})^{1-n}$ such that $P_{\mathrm{c,e}} = 1/\alpha$ and $\lambda = n - 1$.

The few attempts to calculate relative permeability curves following theoretical arguments are all based on Purcell's equation that relates the permeability of a porous medium k to its capillary pressure curve $P_c(S)$ upon conceptualization of the porous medium as bundle of capillary tubes of varying sizes [25], i.e.

$$k \propto \int_0^1 \frac{\mathrm{d}S}{P_c^2(S)} \tag{10}$$

This equation was extended by Gates and Lietz [26] to calculate permeability at partial saturations and further refined by Burdine and coworkers by introducing in front of the integral a so-called tortuosity factor that depends on the fluid saturations [28, 27]. A very similar expression that is more popular within the hydrology community was later derived by Mualem [29]. Burdine (B) and Mualem (M) relationships for the wetting and nonwetting phase relative permeabilities can be generalized to the following expressions:

$$k_{r,w} = (S_w^*)^a \left(\frac{\int_0^{S_w^*} \frac{\mathrm{d}S_w^*}{P_c^2(S_w^*)}}{\int_0^1 \frac{\mathrm{d}S_w^*}{P_c^2(S_w^*)}} \right)^b \quad \text{and} \quad k_{r,nw} = (1 - S_w^*)^a \left(\frac{\int_{S_w^*}^1 \frac{\mathrm{d}S_w^*}{P_c^2(S_w^*)}}{\int_0^1 \frac{\mathrm{d}S_w^*}{P_c^2(S_w^*)}} \right)^b \tag{11}$$

where for the Burdine model $a = 2$ and $b = 1$, while the Mualem approach requires $b = 2$ and uses a as an additional fitting parameter to account for tortuosity. The combination of the Brooks-Corey (BC), Eq. (8), or the van Genuchten (VG), Eq. (9), capillary pressure models with Eq. 11 allow analytical expressions for the relative permeability functions to be obtained (Table 1). It should be pointed out that besides the theoretical models described

TABLE 1. Analytical expressions for the wetting and nonwetting phase relative permeability curves as obtained upon combination of the Brooks-Corey (BC) and van Genuchten (VG) capillary pressure models within the Burdine (B) or Mualem (M) framework.

	Capillary pressure function $P_c(S)$	
	Brooks-Corey (BC)	van Genuchten (VG) $m = n/(n-1)$
Burdine framework	$k_{r,w} = \left(S_w^*\right)^{3+2/\lambda}$	$k_{r,w} = \left(S_w^*\right)^2 \left\{1 - \left[1 - \left(S_w^*\right)^m\right]^{1/m}\right\}$
	$k_{r,nw} = \left(1 - S_w^*\right)^2 \left[1 - \left(S_w^*\right)^{1+2/\lambda}\right]$	$k_{r,nw} = \left(1 - S_w^*\right)^2 \left[1 - \left(S_w^*\right)^m\right]^{1/m}$
Mualem framework	$k_{r,w} = \left(S_w^*\right)^{a+2(1+1/\lambda)}$	$k_{r,w} = \left(S_w^*\right)^a \left\{1 - \left[1 - \left(S_w^*\right)^m\right]^{1/m}\right\}^2$
	$k_{r,nw} = \left(1 - S_w^*\right)^a \left[1 - \left(S_w^*\right)^{1+1/\lambda}\right]^2$	$k_{r,nw} = \left(1 - S_w^*\right)^a \left[1 - \left(S_w^*\right)^m\right]^{2/m}$

above, empirical functions are often used that take the following general form:

$$k_{\mathrm{r,w}} = k^{\mathrm{o}}_{\mathrm{r,w}} \left(\frac{S_{\mathrm{w}} - S_{\mathrm{w,ir}}}{1 - S_{\mathrm{w,ir}} - S_{\mathrm{nw,r}}} \right)^{n_1} \quad \text{and} \quad k_{\mathrm{r,nw}} = k^{\mathrm{o}}_{\mathrm{r,nw}} \left(\frac{1 - S_{\mathrm{w}} - S_{\mathrm{nw,r}}}{1 - S_{\mathrm{w,ir}} - S_{\mathrm{nw,r}}} \right)^{n_2} \tag{12}$$

The advantage of these formulations is that a reasonably good fit of the experimental data is often achieved by proper choice of the values for the end-point relative permeabilities $k^{\mathrm{o}}_{\mathrm{r,w}}$ and $k^{\mathrm{o}}_{\mathrm{r,nw}}$ as well as for the exponents n_1 and n_2 (which independently control the curvature of the relative permeability function) [4].

As anticipated in Section 2.2.3, hysteresis effects are quantified through the amount of nonwetting phase that is trapped upon flow reversal, i.e. from drainage to imbibition. The most widely applied trapping model is by Land [30], which relates the residual saturation $S_{\mathrm{nw,r}}$ (i.e. the amount trapped at $P_{\mathrm{c}} = 0$) to the actual saturation at flow reversal $S_{\mathrm{nw,i}}$ by the following empirical relationship:

$$S^*_{\mathrm{nw,r}} = \frac{S^*_{\mathrm{nw,i}}}{1 + C S^*_{\mathrm{nw,i}}} \tag{13}$$

where $S^*_{\mathrm{nw}} = 1 - S^*_{\mathrm{w}}$, and C is a positive constant known as the Land coefficient, which can be obtained based on experimental data. Note that $C = 0$ represents the case of complete trapping, while for $C \to \infty$ trapping goes to zero. For any value in between, residually trapped gas increases with increasing initial gas saturation. A more flexible model was recently proposed by Spiteri and coworkers in order to capture the non-monotonic behavior that has been observed in pore network simulations [31] and supported by experimental data [32]. The Spiteri model takes the form of a simple quadratic function, i.e.

$$S^*_{\mathrm{nw,r}} = \alpha S^*_{\mathrm{nw,i}} - \beta (S^*_{\mathrm{nw,i}})^2 \tag{14}$$

where α and β are constant parameters determining the initial slope and the curvature of the function, respectively.

A complete imbibition relative permeability curve can be obtained upon application of a parametric interpolation method between the point of flow reversal (at $S_{\mathrm{nw,i}}$) and the corresponding residual saturation ($S_{\mathrm{nw,r}}$), which can be predicted by applying one of the two models described above [35, 20]. A more physically sound hysteresis model was developed by Land to describe scanning relative permeability curves [30]. The model is based on the definition of a *mobile* nonwetting phase saturation $S_{\mathrm{nw,m}}$ in terms of known variables, such as its actual saturation S_{nw} and its residual saturation $S_{\mathrm{nw,r}}$, where the latter can be again found from Eqs. (13) or (14). As described in [30, 33], $S_{\mathrm{nw,m}}$ is obtained from material balances and is given by

$$S^*_{\mathrm{nw,m}} = \frac{1}{2} \left\{ \left[S^*_{\mathrm{nw}} - S^*_{\mathrm{nw,r}}(S^*_{\mathrm{nw,i}}) \right] + \sqrt{\left[S^*_{\mathrm{nw}} - S^*_{\mathrm{nw,r}}(S^*_{\mathrm{nw,i}}) \right]^2 + \frac{4}{C} \left[S^*_{\mathrm{nw}} - S^*_{\mathrm{nw,r}}(S^*_{\mathrm{nw,i}}) \right]} \right\} \tag{15}$$

Once the mobile saturation is known, the imbibition relative permeability of the nonwetting phase $k^{\mathrm{I}}_{\mathrm{r,nw}}$ can be readily obtained as

$$k^{\mathrm{I}}_{\mathrm{r,nw}}(S^{*}_{\mathrm{nw}}) = k^{\mathrm{D}}_{\mathrm{r,nw}}(S^{*}_{\mathrm{nw,m}}) \tag{16}$$

where $k^{\mathrm{D}}_{\mathrm{r,nw}}$ is the corresponding drainage relative permeability curve that can be obtained from any one of the expressions reported in Table 1. A similar procedure was followed to determine the imbibition relative permeability curve corresponding to the wetting phase [30], though it should be emphasized that for systems having a strong wettability preference (to either oil, water or gas), the latter tends to depend solely on its own saturation and hysteresis can often be neglected [2]. Recent experimental data using a water-wet Berea Sandstone show that this might be true also for the *sc*CO_2-brine system [34]. Additionally, the assumption is often made that imbibition relative permeabilities are reversible, i.e. that the same imbibition curve can be followed during the subsequent drainage step until the bounding drainage curve is reached [35, 20].

3. Relative Permeability and the CO_2-brine System

Much of the interest in multiphase flow has been motivated by the petroleum industry, where the concept of relative permeability is key to processes such as water-flooding and enhanced oil recovery. Factors affecting relative permeability of multiphase flow in porous media for the oil-water system were reviewed by *Honarpour* [41] in 1986 and since then there has been relatively little new experimental work published on the oil-water system. More recently, efforts have been renewed in this area with a focus on the CO_2-brine system and the applications of multiphase flow dynamics to subsurface carbon storage in saline aquifers [42]. In this section the discussion is extended as to how rock and fluid properties that are relevant to multiphase flow affect relative permeability, with particular reference to the CO_2-brine system.

3.1. **The CO_2/water system in the subsurface.** There is a finite range of pressure and temperature conditions for which CO_2 storage is considered practical, a detailed discussion of this is provided by *Bachu* [43]. The low end of temperature and pressure is generally taken to be at depths at which supercritical point of CO_2, 31.1°C and 7.38 MPa, is exceeded sufficiently for CO_2 to have a density of $\rho_{CO_2} > 500$ kg/m^3. By assuming a hydrostatic pressure gradient of 10.5 MPa/km, this condition is met at a depth of about 1000 m in a warm basin and at about 3000 m in a cold basin (see Table 2 for additional details) [44]. As will be discussed below, the main peculiarity of the CO_2/water system is that the pressure/temperature conditions at those depths are still relatively close to the critical point of CO_2, in comparison to the critical point of other gases such as nitrogen ($T_c = -147.0$°C and $P_c = 34.0$ bar) or methane ($T_c = -82.6$°C, $P_c = 46.0$ bar). As a result, while the viscosity of CO_2 is comparable to that of a gas, its density is much larger and liquid-like. From an experimental point of view, this means that the CO_2/water system will be characterized by a high mobility (strong viscosity contrast) and by limited gravity segregation effects. The latter is further reduced by the presence of capillary forces, suggesting that gravity segregation will not affect the performance of horizontal core-floods [23].

3.2. **Fluid Thermophysical Properties.** Fluid densities and viscosities play a primary role in flow, and have well known dependencies on the pressure, temperature, and chemical component composition (e.g. mass fraction H_2O) of the fluids. Several models have been developed in the form of equations of state for both brine and CO_2 across the range of pressure, temperature, and salinity that is applicable to CO_2 storage. Additionally, a review of the chemical composition and origins of formation brines is given by *Hanor* [45], the most relevant features being summarized in the following. Salinity varies widely from less than 50 mg l^{-1} to in excess of 400,000 mg l^{-1}; the anion composition of the brines across the entire range of salinity is dominated by Cl^-, while sodium is the dominant cation at salinities below 300,000 mg l^{-1} (Ca^{2+} concentration increases with salinity, becoming the dominant cation above 300,000, where Mg^{2+} and K^+ also becoming significant, if minor, components of the brine). In Figures 2 and 3 the densities and viscosities of brine and

TABLE 2. Density and viscosity values for water, CO_2, N_2 and CH_4 at temperature and pressure conditions for representative deep-cold (depth 3 km, surface temperature 10°C, geothermal gradient 25°C/km), and shallow-warm basins (depth 1 km, surface temperature 20°C, geothermal gradient 45°C/km). In both cases, a hydrostatic pressure gradient of 10.5 MPa/km is assumed.

	Deep cold basin		**Shallow warm basin**	
	Viscosity [μPa.s]	Density [kg/m^3]	Viscosity [μPa.s]	Density [kg/m^3]
Water	378	995	491	998
CO_2	63	740	24	292
N_2	27	253	21	102
CH_4	22	169	15	66

CO_2 are shown as a function of pressure and temperature using correlations developed by *Phillips et al.* [46] and *Span and Wagner* [47], and by *Kestin et al.* [48] and *Fenghour et al.* [49], respectively. Several models also exist describing the mole fraction (solubility) of

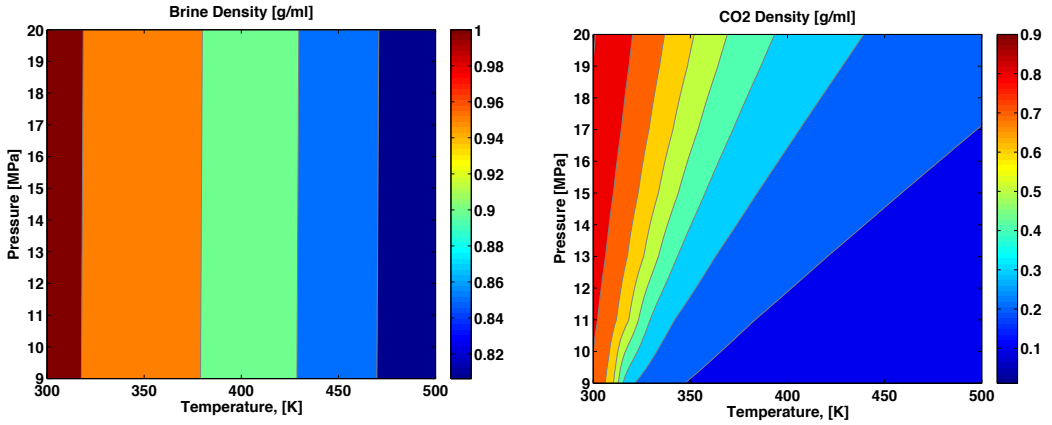

FIGURE 2. Isochores of CO_2 (left) and brine (right) for a range of temperatures and pressures at zero salinity. Correlations by *Span and Wagner* [47], and by *Kestin et al.* [48].

CO_2 in the aqueous phase and H_2O in the CO_2-rich phase for a CO_2-brine system with temperature, pressure, and salinity being the independent variables, the most widely used of which are by *Duan and Sun* [50], *Duan et al.* [51].

For the fluid phases, the interfacial tension of CO_2-brine systems at conditions covering the range relevant to CO_2 storage has been recently measured by a number of groups [52, 53, 54, 55, 56], with the most comprehensive dataset provided by *Li et al.* [56]. As with the single-phase thermophysical properties, the interfacial tension is a function of

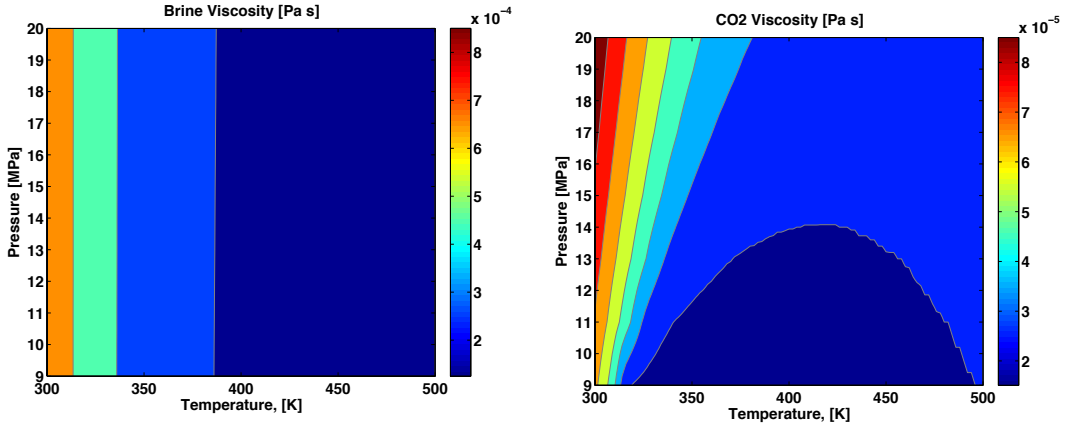

FIGURE 3. Viscosity of CO_2 and brine as functions of pressure and temperature at zero salinity. Correlations by *Kestin et al.* [48] and *Fenghour et al.* [49].

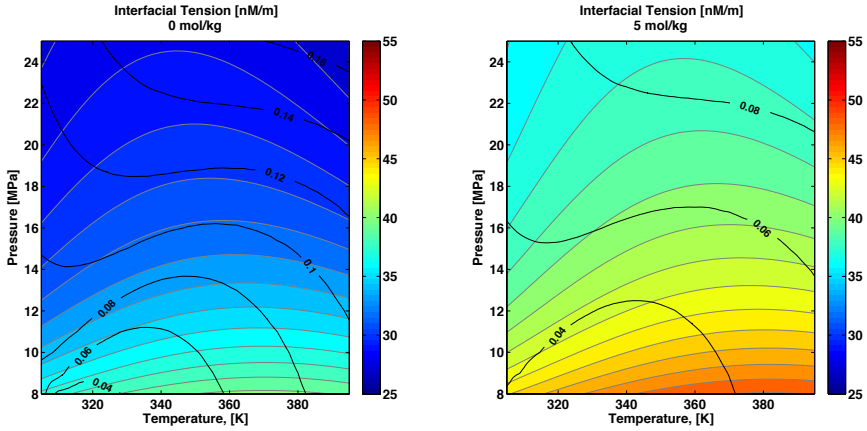

FIGURE 4. Interfacial tension of the CO_2-brine system at 0 and 5 mol.kg^{-1} based on data by *Li et al.* [56]. Lines of constant viscosity ratio shown in black.

pressure, temperature, and brine salinity, generally decreasing with increasing CO_2 solubility. At conditions relevant to subsurface storage, the interfacial tension ranges from 55 mN/m at high temperature, high salinity, and low pressure conditions to 20 mN/m at low temperature, low salinity, and high pressure conditions (see Figure 4). When considering a fluid-rock system, it is crucial to consider the wetting character of the rock, which describes the preferential affinity of one of the fluids to the rock surface. In terms of fluid distribution, the common perception is that the wetting phase preferentially coats the surface of the rock grains, occupying crevices and the smallest pores, while the non-wetting phase exists as droplets in the centre of the pores. Observations for CO_2-brine systems generally

indicate a water-wet system for both sandstone and carbonate mineralogies, but there are contradictory results as to the magnitude of the contact angle and its variation with fluid conditions. *Espinoza and Santamarina* [55] found that the CO_2-brine system is strongly water-wet on quartz and calcite with no impact of changing pressure and a weak dependency on salinity up to 3.5M NaCl. *Chiquet et al.* [52] have also observed the system to be water-wet on quartz with little impact of both pressure and salinity from atmospheric up to 10 MPa pressure and for 0.01-1M NaCl solutions. In mica, however, a transition was observed from water- to intermediate-wet with increasing CO_2 pressure and NaCl and the system appeared to be mixed-wet across the entire range of conditions mica during imbibition (water displacing CO_2). Additionally, in microfluidic experiments with silica micromodels, *Kim et al.* [57] observed contact angles ranging from water- to mixed-wet for the supercritical CO_2-brine system, as the salinity is increased from 0.01-5M NaCl. *Jung and Wan* [58] report a 20° step-change increase in contact angle as the pressure is raised beyond the critical pressure, but little change with increasing pressure is observed beyond this point. Additionally, a systematic increase of 4° per 1M increase in ionic strength (irrespective of the pressure) was observed in the same study.

3.3. **The impact of thermophysical properties on relative permeability.** The primary, independent controls on multiphase flow, other than the rock structure, are pressure, temperature and salinity. These, in turn, affect fluid properties such as viscosity, density, contact angle and interfacial tension and, as such, can be described as secondary variables. Irreducible water and residual CO_2 saturations together with relative permeability may be considered as tertiary variables, as these are in turns controlled by the fluid properties [59]. While it might be straightforward to describe how fluid properties change with pressure, temperature and salinity [48, 49, 50, 56], the design of an experiment where the individual contribution can be identified of each fluid property on the relative permeability represents a challenging exercise. As a result, much of the analysis in the literature relates these effects to dimensionless parameters that combine several variables. One of this lumped parameters is the so-called capillary number, which describes the ratio of viscous (governing flow) to capillary forces (governing trapping) acting in the pore space, i.e.

$$N_c = \frac{q\mu}{\gamma}, \tag{17}$$

where q is the Darcy velocity, μ is the viscosity of the invading fluid and γ the interfacial tension. *Fulcher et al.* [60], *Amaefule and Handy* [61], and *Bardon and Longeron* [62] show that in two-phase systems, the capillary number only has an impact on the shape of the relative permeability curves at values of $N_c > 10^{-6}$ (see also Figure 5). While high capillary number displacements are relevant for certain enhanced oil recovery processes in which the goal is to reduce the interfacial tension between displacing and displaced fluids to a value of less than 1 mN/m, they are not relevant for CO_2 sequestration in which the capillary number will typically be $N_c << 10^{-6}$. In the following sections, the impact of the viscosity ratio, interfacial tension and wettability on relative permeability are discussed in more detail.

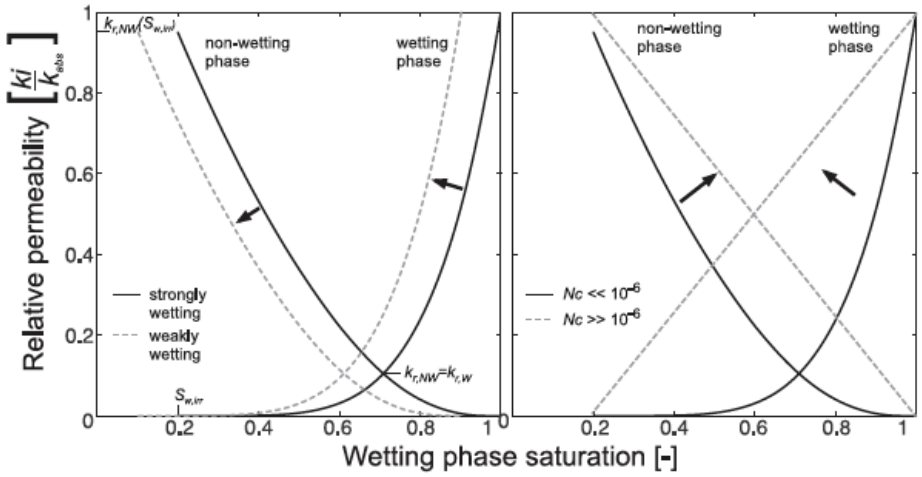

FIGURE 5. Impact of decreasing wettability (L) and increasing capillary number (R) on drainage relative permeability curves [23, 16].

3.3.1. *Viscosity ratio.* The viscosity ratio is defined as the ratio of the viscosity of the non-wetting phase to the wetting phase, where

$$M = \frac{\mu_{\mathrm{nw}}}{\mu_{\mathrm{w}}}. \tag{18}$$

The effect of viscosity ratio on relative permeability is not clear, as experimental observations that are reported in the literature are partly contradictory. For instance, relative permeability has been shown to be both independent of [13] or to increase with M [63, 64, 65] for experiments with oil/water systems. In contrast, *Lefebvre du Prey* [66] shows that for a high viscosity ratio, the relative permeability of the lower viscosity fluid is significantly reduced during drainage. Additionally, *Downie and Crane* [67] find that a subsequent decrease in viscosity ratio does not return the relative permeability to its original value, thus confirming that M is not the sole contributor to changes in relative permeability. For the CO_2-brine system, *Bachu and Bennion* [59] suggest that an increase of IFT or a decrease in the viscosity ratio leads to similar changes of $k_{\mathrm{r,w}}$, $S_{\mathrm{w,ir}}$ and $S_{\mathrm{CO_2,r}}$, with relative permeabilities increasing and residual saturations decreasing. They suggest that as the viscosity ratio increases, the less viscous or more mobile fluid will be more able to flow through the pore space, but they also highlight that from those experiments the individual effects of IFT and M cannot be separated. As discussed in section 3.2, the viscosities of CO_2 (μ_{CO_2}) and brine (μ_b) increase with increasing pressure and decreasing temperature [49], and μ_b increases with increasing salinity [68]. Additionally, μ_{CO_2} is always much less than μ_b, and viscosity ratios from 0.02 to 0.2 are expected at geologically relevant conditions (Figure 6) [44]. Most importantly, in the CO_2-brine system and at constant brine salinity, most of the changes in M come from changes in μ_{CO_2} (Figure 3), with M generally increasing with increasing pressure and temperature, while at constant pressure and temperature conditions

but varying salinity, the change in M comes exclusively from μ_{b}. In either case, we expect the magnitude of these changes on the relative permeability to be small, as flow at the core-scale is dominated by capillary forces ($N_{\mathrm{c}} < 10^{-5}$) and the position of fluid interfaces will be dominated by IFT and P_c.

There are two contexts in which the question of the influence of the viscosity ratio is relevant. First, if the relative permeability is a strong function of the viscosity ratio, then it would be important to make the measurements at conditions representative of the specific storage project to which the relative permeability curves would be applied. Second, if at a particular storage site the viscosity ratio changed significantly over time for for different parts of the plume, for example near the injection well as compared to far from it, then it may be necessary to include a viscosity ratio dependent relative permeability for predicting the performance of a storage project. Regarding the latter, while in interesting academic question, it is unlikely to be necessary because the pressure and temperature are likely to remain within about 10

3.3.2. *Interfacial Tension.* The majority of published work investigating the effect of interfacial tension (IFT) on relative permeability is focussed on enhanced oil recovery, where the aim is to reduce the oil/water IFT through the injection of surfactants to the extent that the flow approximates miscible behavior. Although a small but measurable increase in relative permeabilities is reported for the oil/water system in unconsolidated sand for IFTs of 5 to 40 mN/m with decreasing IFT [13, 69, 70], little or no change is seen in consolidated media, where very low IFTs ($\sim 10^{-3}$ mN/m) are typically required to observe a significant effect on the relative permeability and accordingly on residual saturations. For instance, *Bardon and Longeron* [62] find a linear increase in $k_{r,o}$ with IFT decreasing from 12.6 to 0.065 mN/m for the gas-oil system; the effect is much larger for $\gamma < 0.04$ mN/m, below which the relative permeability curves straighten and residual saturations tend to zero. For the oil-water system, *Amaefule and Handy* [61] report similar trends for both relative permeability and residual saturation at low IFT (10^{-1} mN/m or less), while no changes have been observed for $\gamma > 1$ mN/m. Similarly, *Fulcher et al.* [60] find an significant increase in relative permeabilities for IFTs below 2 mN/m and no changes above 5.5 mN/m. Interestingly, *Batycky and McCaffery* [70] indicate that imbibition relative permeability curves are more significantly affected by lowering IFT than drainage curves.

Interfacial tensions for the CO_2-brine system range from 25 to 55 mN/m at the conditions for subsurface storage (Figure 4). As described above, observations for the oil-brine system suggest that for these high interfacial tensions there is a negligible effect on the relative permeability curve. However, data available in the literature for the CO_2-brine system, albeit limited in number, lead to opposite conclusions. In particular, *Bennion and Bachu* [71] measured drainage and imbibition relative permeability curves for IFTs in the range 19.8 to 56.2 mN.m^{-1} in a water-wet sandstone. Unlike the oil-brine system, a significant increase in $k_{\mathrm{r,w}}$ and $k_{\mathrm{r,nw}}$ is observed for decreasing IFT. Additionally, the imbibition curves become more linear with decreasing IFT, suggesting there is an increase in total relative mobility and the behavior at low IFT approximates miscible flow [72]. Also, endpoint

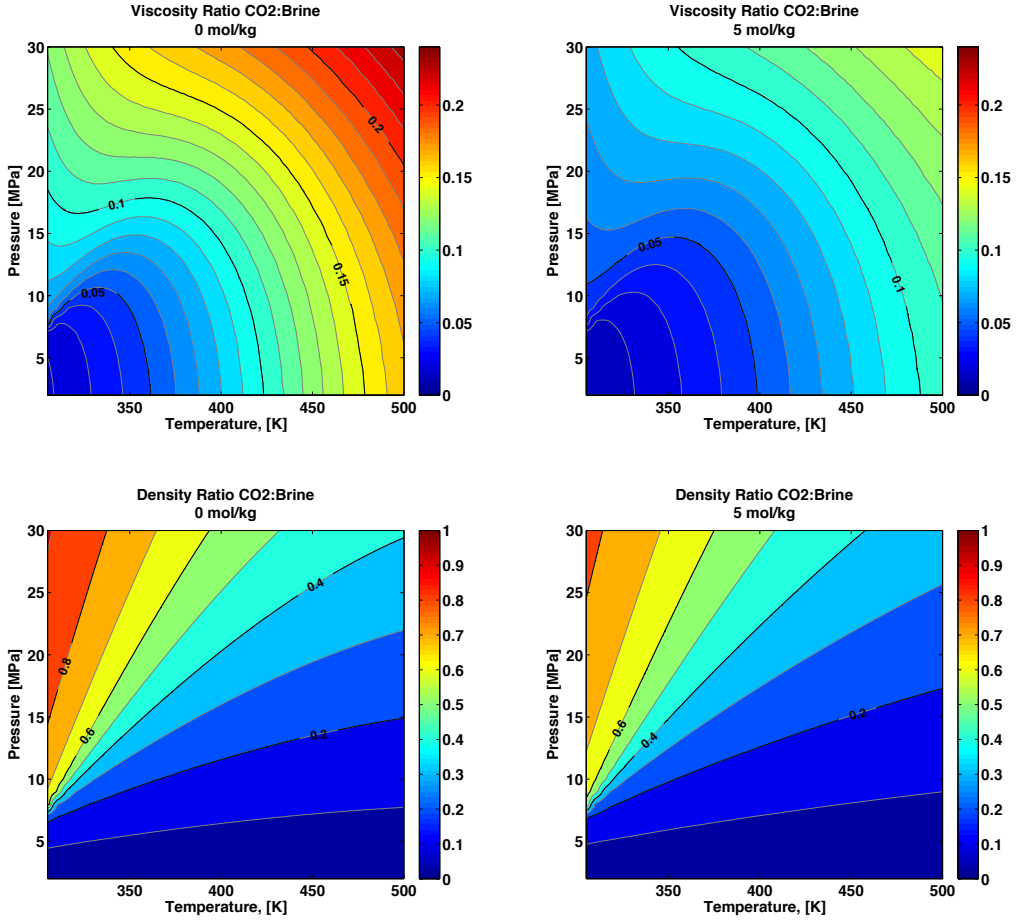

FIGURE 6. Viscosity and density ratios of CO_2 with respect to brine as functions of pressure and temperature at salinities of 0 mol kg^{-1} and 5 mol kg^{-1}.

k_{r,CO_2} and $S_{CO_2}^{max}$ both increase as IFT decreases [72, 73]. However, as previously noted by the same authors, the effects of viscosity ratio and IFT cannot be separated for this particular experimental campaign, as the viscosity ratio simultaneously (and significantly) increases (M=0.02, 0.05 and 0.1) as IFT decreases (γ=56, 34, 20 mN/m). The discrepancy between the observations of [72] and previous studies about the influence of IFT could also potentially be explained by the low viscosity ratio of the CO_2-brine system ($<<1$) as compared to the high viscosity ratio of the oil-water system ($>>1$). In general, the oil-water system is much more strongly controlled by viscous forces, which have have the effect

of decreasing the influence of IFT on distribution of the wetting and non-wetting fluids. More about this topic is provided in discussion.

3.3.3. *Wetting.* The wettability of oil reservoirs varies widely from strongly water-wet to strongly-oil wet including situations where the same reservoirs presents both oil or water-wet regions (mixed-wet system). In this context, the wetting properties of the reservoir are considered to exert the greatest control on the fluid flow behavior and eventually on the amount of recoverable oil [74]. Endpoint relative permeability values after drainage and imbibition can be thought of as qualitative measures of wettability and the following generalizations have been observed for hydrocarbon/water systems [16]. For systems with a well-defined wettability preference, irreducible wetting phase saturation after drainage is in the range $S_{\mathrm{w,irr}} > 20\%$, wetting and nonwetting phase relative permeabilities are equal at a wetting-phase saturation of $S_{\mathrm{w}} > 50\%$, and the maximum relative permeability of the nonwetting phase during drainage is in the range $k_{\mathrm{r,nw}}(S_{\mathrm{w,irr}}) = 50 - 100\%$. Thus, for a water-wet reservoir is not surprising that the endpoint relative permeability to water after imbibition will be smaller than the relative permeability to the nonwetting phase after drainage, as the nonwetting phase presents more of a barrier to flow of the wetting phase than the wetting does to flow of the non-wetting, the latter occupying mostly the centre of the pores. With respect to intermediate or mixed-wet systems, the relative permeability of a particular phase tends to decrease with increases in rock wetting with respect to that phase [75], although this has been disputed by *Dullien* [2]. Additionally, hysteresis in the relative permeability is more prominent in the nonwetting phase and very minor in the wetting phase, with $k_{\mathrm{r,nw}}$ for imbibition being less at a given saturation [76, 14]. With decreasing wettability, hysteresis will be apparent in both wetting and non-wetting phase relative permeability curves [14].

For CO_2 storage in sandstone saline aquifers, the reservoirs under consideration are expected to be predominantly water-wet [55, 57, 58]. Core-flood experiments with CO_2 and brine also indicate strongly water-wet behaviour for siliciclastic rocks [22, 23] and classic hysteresis behaviour is observed, where $k_{\mathrm{r},i}$ is greater for S_i increasing rather than decreasing [73].

4. The use of relative permeability in flow problems

The concept of relative permeability was developed as a necessary input to mathematical models that describe the motion of multiple fluid phases flowing through reservoir rocks at scales where observation is not practical [7]. Reservoir simulation is now an integral part of a variety of problems of multiphase flow in natural settings, from groundwater remediation in shallower aquifers to the production of oil and gas from deep underground reservoirs [77].

Equations of motion are typically partial differential equations that combine an expression of mass conservation with constitutive relationships, i.e. empirical relationships between a force applied to a fluid and the response of that fluid in terms of pressure, temperature and motion. In this context, capillary pressure and relative permeability curves are constitutive relationships correlating the pressure and permeability of a fluid phase with saturation. When coupled to a conservation of mass for each phase and appropriate boundary and initial conditions, a problem is fully specified. If the equations can be solved using analytical or numerical techniques, a unique description of fluid flow in that system will be obtained.

It is here that the true nature of relative permeability is revealed. On the one hand, many constitutive relationships, e.g., Darcy's law for single-phase flow, have been shown under appropriate conditions to be exact continuum-scale descriptors of the average of smaller scale physical processes. On the other hand, the relative permeability-saturation relationship has been shown to be at best an approximate description of the aggregate impact of multi-fluid displacement at the pore-scale [2]. By definition, hysteresis in the $k_r - S$ relationship indicates that saturation does not uniquely determine the relative permeability of a rock to a given phase. Models that incorporate independent variables other than the saturation (such as the interfacial area, [37, 38]) have been proposed, but not widely adopted. In the following, the flow equations are presented followed by their solution using the Buckley-Leverett approach for flow in one dimension. This is used to illustrate the impact of relative permeability on multiphase flow. Additionally Buckley-Leverett theory underpins the most commonly used technique for measuring relative permeability, as is discussed in detail Section 5.

4.1. **The basic flow equations.**

The CO_2-brine system is a two-phase system ($N_p = 2$) where the CO_2 - and a water - rich phases are considered non-wetting (nw) and wetting (w) respectively. Ignoring changes in thermophysical properties (assuming fluids are incompressible and immiscible), the basic equations of flow in one dimension are given by mass balance equations and constitutive relationships. The mass balance equations are as

follows:

$$\phi \frac{\partial S_{\mathrm{w}}}{\partial t} + \frac{\partial q_{\mathrm{w}}}{\partial x} = 0 \tag{19}$$

$$\phi \frac{\partial S_{\mathrm{nw}}}{\partial t} + \frac{\partial q_{\mathrm{nw}}}{\partial x} = 0 \tag{20}$$

$$S_{\mathrm{w}} + S_{\mathrm{nw}} = 1. \tag{21}$$

The constitutive relationships include Eq.(7) for the flow velocity as a function of pressure and saturation, together with the capillary pressure characteristic function, $P_{\mathrm{c}}(S_{\mathrm{w}}) = P_{\mathrm{nw}} - P_{\mathrm{w}}$. Substituting for q_i as given by Darcy's law, Eq.(7), into the mass balance equation results in

$$\phi \frac{\partial S_i}{\partial t} - \frac{\partial}{\partial x}\left(k \lambda_i \frac{\partial \Phi_i}{\partial x} \right) = 0 \qquad i = 1, ..., N_{\mathrm{p}} \tag{22}$$

where

$$\lambda_i \equiv \frac{k_{\mathrm{r},i}}{\mu_i} \qquad i = \mathrm{nw}, \mathrm{w}. \tag{23}$$

In this formulation there are four equations and four unknowns, $S_{\mathrm{w}}, S_{\mathrm{nw}}, P_{\mathrm{w}}, P_{\mathrm{nw}}$, and the independent variables are time, t, and space, x. Eq.(22) is a second order non-linear partial differential equation and it generally must be solved using numerical techniques. There are a number of special cases, however, when there exists a closed form solution to the flow equations. The most widely used case is the *Buckley and Leverett* [39] solution for 1-D immiscible displacement, presented in the next section.

4.2. **The Buckley-Leverett solution for forced displacement.** The most widely used analytical solution to the 1-D flow equations is the Buckley-Leverett solution for forced displacement [39]. Under certain circumstances, this type of displacement closely approximates core-flood experiments in the laboratory and for this reason Buckley-Leverett theory underlies the most widely used technique for deriving relative permeabilities from core floods (see Section 5). In addition, it can be used for first-order approximations of horizontal or vertical flow at the field-scale and in general the equations are useful for demonstrating the impact of fluid properties and relative permeability on multiphase flow.

4.2.1. *The fractional flow formulation.* The fractional flow formulation is used to reduce the number of dependent variables in the flow equations from four to two, $S_{\mathrm{w}}, S_{\mathrm{nw}}$, and to reduce the problem from a second-order non-linear PDE to a first order quasi-linear PDE, which can be solved analytically.

Consider again the displacement of water (w) by CO_2 (nw) with flow limited to one dimension. Assume, additionally, that the CO_2 and water phases are equilibrated with each other such that they can be considered immiscible. Let the fractional flow of CO_2 be defined by

$$F_{\mathrm{nw}} \equiv \frac{q_{\mathrm{nw}}}{q_{\mathrm{nw}} + q_{\mathrm{w}}} = \frac{q_{\mathrm{nw}}}{q_{\mathrm{t}}} \tag{24}$$

where q_t is the total volumetric flow rate, $q_t = q_{nw} + q_w$. By making use of Eqs.(7) as well as of the definition of capillary pressure, one can obtain an expression for the effective flow rate of CO_2 in terms of viscous, capillary and gravity driven flow,

$$F_{nw} = \frac{\lambda_{nw}}{\lambda_t} - \frac{k}{q_t}\frac{\lambda_w\lambda_{nw}}{\lambda_t}\frac{dP_c}{dS_w}\frac{dS_w}{dx} - \frac{k}{q_t}g_x\frac{\lambda_w\lambda_{nw}}{\lambda_t}(\rho_{nw} - \rho_w). \tag{25}$$

The three terms on the right hand side of Eq.(25) represent the contribution to flow from viscous, capillary, and gravitational driving forces, respectively. The key attribute of the fractional flow formulation that makes it useful in simplifying flow problems is that fractional flow can be shown to be a function of saturation only, i.e. $F_i(S_i)$, and it directly depends on the extent to which viscous, capillary and gravity potentials contribute to driving the flow. Additionally, the relative permeability-saturation relationship for both phases is present in all three terms of the right hand side of Eq.(25) and it therefore directly determines the nature of the fractional flow-saturation relationship. Most importantly, the functional form of the fractional flow-saturation relationship will in turn affect rates and character of the displacement processes.

4.2.2. *The Buckley-Leverett solution.* The Buckley-Leverett theory applies to immiscible fluid flow in 1-D and assumes that the capillary potential is negligible as compared with viscous or gravitational drives. In a laboratory core-flood, this is achieved upon injection of fluids at sufficiently high flow rates so that the second term in Eq.(25) can be ignored. In horizontal core-floods the gravitational term also drops out of the equation and one is left with a reduced fractional flow function,

$$F_{nw} \approx f_{nw} = \frac{\lambda_{nw}}{\lambda_t}. \tag{26}$$

The flow equation can now be formulated as a quasi-linear first order partial differential equation with S as the only dependent variable. For the nonwetting phase we can therefore write

$$\frac{\partial S_{nw}}{\partial t_D} + \frac{df_{nw}}{dS_{nw}}\frac{\partial S_{nw}}{\partial x_D} = 0. \tag{27}$$

where the following dimensionless variables have been introduced, namely $x_D \equiv x/L$ and $t_D \equiv \int_0^t q dt/(\phi L)$, with L being a characteristic length, e.g., the length of a core. This equation is a first-order quasi-linear PDE and it can be solved using the method of characteristics. In particular, Eq.(27) can be decomposed in two equations that fully describe the solution of the problem, i.e.

$$\frac{dS_{nw}}{dt_D} = 0 \tag{28}$$

$$\frac{dx_D}{dt_D} = \frac{df_{nw}}{dS_{nw}} \tag{29}$$

Typically, the solution is given by so-called characteristic curves that can be drawn on a $t_D - x_D$ plane: along each characteristic the saturation is constant ($dS_{nw}/dt_D = 0$) and the

characteristics are straight lines with slope $dS_{\rm nw}/df_{\rm nw}$. In other words, a given saturation will propagate at a constant velocity $f'_{\rm nw} = df_{\rm nw}/dS_{\rm nw}$ through the porous medium, this velocity being dependent on the relative permeability and viscosity of the fluids (through Eqs.(23) and (26)).

4.3. **A Practical Example: Oil or CO_2 Injection Into a Water Saturated Core.** Consider a core-flooding experiment where a nonwetting phase (oil or CO_2) and a wetting phase (water) are co-injected at a fractional flow corresponding to the irreducible wetting phase saturation ($S_{\rm nw} \approx 0.4$) into a core initially saturated with wetting phase. Let's further assume that the wetting and nonwetting phase relative permeability functions are Brooks-Corey curves of the form shown in Figure 7. The corresponding fractional flow curves are shown for four different viscosity ratios ($\mu_{\rm w}/\mu_{\rm nw} = 0.1, 1, 10, 100$). Given this information, the system is fully characterized and Eq.(28) provides the solution to this problem as depicted by the characteristic plane shown as the right panel of Figure 7 for a viscosity ratio $\mu_{\rm w}/\mu_{\rm nw} = 0.1$. From the figure, it can be seen that the injection of about 0.5 pore volumes is required to observe breakthrough at the effluent end of the core ($x_{\rm D} = 1$). After that the saturation of CO_2 steadily increases and approaches the injection composition after about 7.5 pore volumes have been injected. The saturation at which the injection front propagates is known as the shock front in the Buckley-Leverett formulation. The shock saturation is given by the value of saturation at the point where the derivative of the fractional flow function, $df_{\rm nw}/dS_{\rm nw}$, is equal to the slope of the line extending from the initial saturation to the fractional flow curve (Figure 7). For CO_2/water systems, as with other systems with low mobility ratios, this saturation is typically very low and this has important implications for the design and interpretation of experiments aimed at measuring relative permeability curves.

Figure 8 illustrates the role of viscosity ratio on the performance of the core-flood for the same simulated experiment described above. In the figure, the required injected pore volume to observe breakthrough (A) and to reach a saturation very close to the endpoint ($S_{\rm w,irr} \approx S^*_{\rm w} = 0.4$) (B) are plotted as a function of the viscosity ratio together with the range of saturation observed at the outlet of the core (C). The following conclusions can be made based on these results. The displacement of water by the a less viscous fluid (such as CO_2) leads to a poor sweep efficiency. On the one hand, horizontal core-floods with a high (unfavorable) mobility ratio are expected to give the best results for all those experimental methods that are based on effluent fractional flow data, as these experiments are characterized by an early breakthrough of the injected fluid and accordingly by a broad range of saturation (and therefore relative permeability) that can be measured at the effluent end [40]. On the other hand, an unfavorable mobility ratio may result in an impractical amount of time (pore volumes of fluid injected) before a useful saturation range is covered and the end-point reached (200-3000 PVI in Figure 8B for viscosity ratios relevant for CO_2 sequestration).

These considerations highlight that the behaviors observed during multiphase displacement are directly controlled by the shape of the fractional flow curve, which is a strong function of

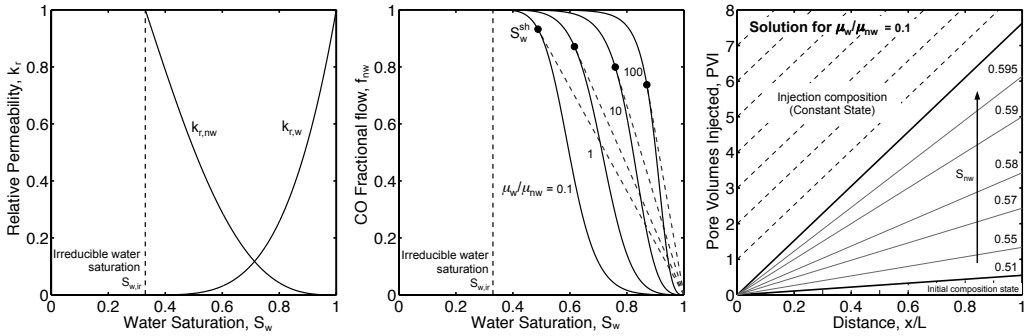

FIGURE 7. Interpreting a core-flood experiment through the method of characteristics: injection of a nonwetting fluid into a core completely saturated with the wetting fluid (water). Brooks-Corey curves are assumed for the relative permeability function and the corresponding fractional flow curves are shown for different viscosity ratios ($\mu_{\rm w}/\mu_{\rm nw}$=0.1-100). An example of solution depicted on the $t_{\rm D} - x_{\rm D}$ plane is shown for the case $\mu_{\rm w}/\mu_{\rm nw}$=0.1.

the relative permeability curve. As presented in the previous section, the latter is affected by both the thermophysical properties of the fluids involved and by the petrophysical characteristics of the rock.

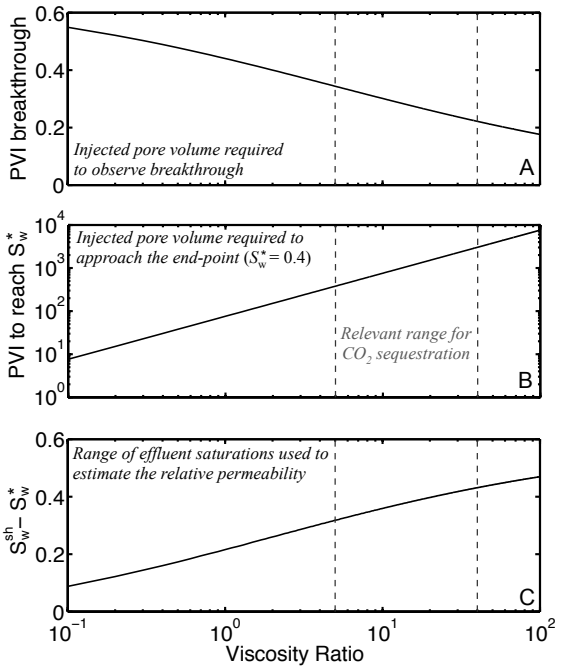

FIGURE 8. Design parameters related to the measurement of relative permeability curves with the CO_2/Water system.Panel A illustrates that the CO_2 saturation at breakthrough during a coreflood experiment will be from 0.2 ot 0.4. Panel B illustrates that from 200 to 3000 pore volumes will need to be injected to approach the end point saturation. Panel C illustrates the range of saturations that can be used to calculate relative permeability during injection of 100% of the non-wetting fluid.

5. Measurement of relative permeability

5.1. **Assumptions Behind Using Core Tests for Deriving Field Properties.** The application of core analysis to provide data for reservoir characterization is a research field under continuous development as new challenges are faced and novel technologies are developed. One of the main challenges is accounting for the heterogeneous nature of reservoir rocks [78]. Not only is it important to quantify the degree and nature of the heterogeneity of rock samples, but also, to make measurements for the full range of rock types present in a reservoir. Ideally, enough samples should be chosen to cover the entire range of rock properties evident in the formation; in this context, multidimensional scanning techniques, such as x-ray Computed Tomography (CT) or Nuclear Magnetic Resonance (NMR) imaging, are increasingly being used for core screening to assist sample selection and to obtain additional diagnostic information about rock heterogeneity and saturation distribution [79, 80, 121]. Additionally, since the scale of the local heterogeneity that can be observed is directly proportional to the dimensions of the given sample, measurements on whole-cores (about 15 cm length and 4.4 to 13.3 cm diameter) should generally be preferred to those on sample's plugs (typically 2.5 to 3.8 cm in diameter and 5 cm long) [78].

In addition to the petrophysical properties, the nature of flow in a porous medium is determined by the interactions with the fluids (i.e. interfacial and adsorption phenomena, chemical reactions, etc.) and by the interplay of the forces involved in the displacement process [81]. This implies that to provide reliable estimates for these parameters for field scale predictions, measurements should be taken at conditions representative of those found in the reservoir. Knowledge of the mineralogy of the rock is highly recommended before embarking on a lengthy core study, particularly when sensitive minerals such as clays are be present [80]. Representative fluids should be used in the core-flooding experiments, so as to establish similar wettability conditions as in the reservoir. Relative permeability tests conducted at analogue conditions (including pressure, temperature and fluids) can also be useful, provided that their reliability is supported by comparison with a sufficient number of tests performed under simulated reservoir conditions [79].

The flow regime established in the reservoir at a given operating condition ultimately control the fluid distribution within the reservoir, thus affecting its performance [81]. This is determined by the relative magnitudes of viscous, capillary and gravity forces, and ideally, the core-flooding experiment should be carried out in such a way that the similarity in the microscopic flow behavior between the reservoir and the core is maintained [79]. Although a quantitative characterization of displacement process at the pore scale is essential for the understanding of multiphase flow in porous rocks, this approach can hardly lead to a complete and useful description of the dynamics of large floods [82]. This analysis should be based on equations of motion that are applicable to the continuum scale, thus involving the generalization of Darcy's law to relative permeabilities [85]. Through a dimensional analysis of these equations, relevant terms (or scaling groups) are identified, which can be used to design experiments in the laboratory [81, 83]. In that respect, scaling criteria

for core-flooding experiments have been introduced, so as to reproduce a situation where the capillary pressure gradient in the direction of flow is small compared to the imposed pressure gradient [84], a situation which is typically encountered in a reservoir, where viscous and buoyancy forces dominate, especially in the region close to the production or injection wells [82]. Since at the pore scale fluid distribution is controlled by capillarity, this requires the application of much higher flow rates in a core-food than those encountered in a reservoir [84]. Furthermore, this type of approach was proven to be effective in describing both gravity- and capillary-dominated displacements in homogeneous reservoirs as wells as in systems with with simple forms of heterogeneity (such as layered reservoirs) [81].

It should also be emphasized that the use of imaging techniques such as CT scanning have provided a new level of observational detail not previously available to early investigators into the effects of heterogeneity on relative permeability and saturation distribution [86]. CT scanning allows for the observation of sub-core scale saturation and porosity distributions within a rock core at any time during a core-flooding experiment; accurate measurement of these properties is typically achieved at a resolution of $\sim$6 mm^3 and above, a volume that exceeds the size of a Representative Elementary Volume (REV) for most sandstones [87, 88]. This allows therefore for the application of the scaling approaches just described to core flooding experiments, thus setting a platform where methods can be developed and tested for up-scaling continuum scale properties, such as capillary pressure and relative permeability curves.

5.2. **Steady-state tests for relative permeability.** Steady-state tests of relative permeability depend on creating a steady-state saturation of fluid phases within a core and measuring the permeability to one or both phases while this saturation is maintained. If the relative permeability-saturation function is the same for all parts of the core (i.e. a homogenous sample), then it is evident from equation 7 that the pressure gradient in the core will only be constant if the saturation of each phase is constant throughout the core (i.e. $S_i(x) = constant$). In this case, the capillary pressure will be constant throughout the core, the pressure gradient will be equal for each phase, $\frac{dP_i}{dx} = \frac{dP}{dx}$, and Eq. 7 is simplified to

$$q_i = -\frac{Akk_{\mathrm{r},i}(S_i)}{\mu_i}\frac{\Delta P}{L}. \tag{30}$$

Relative permeability is obtained by circulating CO_2 and/or water through the core at controlled flow-rates, observing the pressure drop across the core, and measuring the saturation through x-ray CT, weighing the pressure vessel containing the core or using mass balance and precise measures of the water production history.

The most common variations of the steady-state technique are the so-called single-sample dynamic method and the Penn-State technique [79, 89]. In both methods fluid phases are co-injected with the total volumetric flow rates ($q_{CO_2}+q_{\mathrm{water}}$) maintained constant. Carbon dioxide saturation is incrementally increased from zero in a drainage (CO_2 displacing water) process by simultaneously increasing the relative volumetric flux of CO_2 and decreasing

the relative flow of water. At each stage that the CO_2 flow is increased, injection continues until an equilibrium saturation is achieved in the core. This saturation corresponds to the saturation given by the fractional flow curve. The methods only differ in how they minimise the impact of capillary end effects (see section 5.4.1). The dynamic method uses injection rates high enough such that the end-effects are limited to a small region at the boundaries of the core. In the Penn-state method the pressure measurements are made in the central part of the core away from the boundaries of the porous medium so that capillary end-effects have minimal impact on the observations [89, 90]. Less commonly used methods are reviewed by *Honarpour and Mahmood* [79] and often include the use of semipermeable membranes in configurations that allow for the maintenance of a constant capillary pressure across the core while at least one fluid phase is flowing.

5.3. **Unsteady Methods.** Unsteady methods for measuring relative permeability include both core-flooding and centrifuge experiments [79]. A typical unsteady experiment consists of injecting a single-phase into a core initially saturated with the phase to be displaced. Depending on the application, the initial conditions might be at 100% saturation of the fluid to be displaced or at the irreducible (residual) saturation of the displacing fluid. In a core-flooding experiment, the displacement is carried out at either constant rate or constant pressure, while continuously monitoring pressure differential across the core together with cumulative injected and effluent volumes [91, 92]. In a centrifuge experiment, the required pressure differential is developed upon rotating the sample at large speeds and the displacement is carried out under the action of gravity drainage. Also in this case fluid production is measured as a function of time, but only the relative permeability to the invading phase can be obtained [93, 94, 40, 79, 92]. Irrespective of the technique used to obtain the pressure and flow data, relative permeability curves are obtained by applying a given mathematical model that describes the experimental observations. Since the latter typically consist of effluent fractional flow data, the measured relative permeability curve is in principle restricted to the range of saturation values observed after breakthrough of the injected phase. The simplest version of such a mathematical model is given by the well-known Buckley-Leverett equation: the so-called Welge [95] and JBN [96] methods, for the core flooding experiments, and the Hagoort method [94] for the centrifuge experiments belong to this category. Like the steady state method, the applicability of these approaches is constrained by the assumptions behind the Buckley-Leverett equation: fluids are assumed to be incompressible and immisicible, flow is perfectly dispersed, and both gravity and capillary effects are negligible [91]. From a practical perspective, the latter condition is achieved upon injection at high flow rates, which might however lead to severe problems with fines mobilization and viscous instability effects [91, 92]. Additionally, the analysis requires differentiation of the volume data to determine the flow rate of each phase and when working with heterogeneous cores, this might lead to significant errors in the computed relative permeability curve if the data are not properly smoothed [98]. At the same time, the strength of these methods lies in their simplicity, as relative permeability curves are directly obtained from a graphical representation of the experimental data that is based on the method of characteristics [4]. In fact, very useful insights can be

gathered from such an analysis with relevance to the measurement of relative permeability curves with the unsteady technique that are generally valid, thus including the CO_2-brine system. For instance, the injection of CO_2 into a brine saturated core is characterized by an unfavorable viscosity ratio ($\mu_{nw}/\mu_w \approx 0.02 - 0.2$); as explained in Section 4.2, this leads to a poor sweep efficiency and longer experiments, contrary to the common perception that unsteady methods are quicker than steady-state methods.

5.3.1. *Recent developments.* With the aim of relaxing the assumptions imposed by the Buckley-Leverett theory, more complex mathematical models are now applied to the measurement of relative permeability curves from both core-flooding and centrifuge experiments. The general concept behind this approach is that relative permeability curves are adjusted so that, when used to simulate the core-flood experiment mathematically, the computed pressure drop and production match the measured data [97]. The application of this history matching technique was first reported by *Archer and Wong* [98] and refined by subsequent studies where oil/water relative permeability curves have been determined from displacement data on various sandstone and carbonate reservoir cores [99, 84, 100]. In an analogous way, the works by *Firoozabadi and Aziz* [101] and by *Hirasaki et al.* [102] report estimation of relative permeability curves from centrifuge data. It is worth highlighting that the mathematical equations used to describe core-flooding and centrifuge experiments are essentially the same, the main differences residing in the acceleration term in Darcy's law and in the applied boundary conditions [92]. From a practical point of view, the same reservoir simulators are applied that are used to predict performances in the field and that can account for both gravity and capillary pressure effects; this is important, as experiments can be carried out at lower (and more representative) flow rates and end-effects (see below) can be properly accounted for. Typically, a specific functional relationship is assumed for both relative permeability and capillary pressure functions(for example, the types of functions described in Section 2.3, and the corresponding parameters are then adjusted to obtain the best fit the production data. To this aim, a power-law formulation is often applied to both capillary pressure and relative permeability curves with independently fitted parameters [99, 84, 100, 101, 102]. To allow for more flexibility in the shape of the estimated relative permeability curves, the use of cubic splines has also been proposed, though usually this requires the imposition of additional constraints to ensure that the curve remains convex downward and monotonic [103]. With respect to the CO_2-brine system, *Bachu and Bennion* [59] provide a comprehensive data set for approximately 20 unsteady relative permeability tests on sandstone and carbonate core samples across a range of pressures, temperatures, and brine salinity, and where a Brooks-Corey type of relationship was assumed. It should also be emphasized, the coupling with a reservoir simulator is very helpful as it provides a complete history match over the entire range of saturation change, regardless of the fractional flow characteristics of the displacement [91]. As a matter of fact, this approach would become very powerful if coupled to imaging technique that provide direct observation of saturation distribution within the core sample, though to the authors' knowledge, this has not been reported yet for unsteady techniques.

Beside the essential premise of good laboratory data, the success of the implicit history-matching technique just described resides in the appropriate representation of both capillary pressure and relative permeability curves [103, 97]. On the one hand, although capillary pressure can be parameterized when using numerical simulations to derive relative permeability curves, some studies have neglected it [100, 103], thus leading to significant errors [84]. On the other hand, even if both curves are properly parametrized, the estimated relative permeability curve might be biased by the selection of the given functional form for the two properties [103] and the solution might therefore not be unique [101]. Additionally, so-called modeling errors can arise from an inaccurate description of the flow processes, such as when reservoir cores are assumed to be homogeneous and one-dimensional [103]. Although the influence of heterogeneity on relative permeability has been recognized for a very long time (see the work by Krause for an extensive review on this topic [86]), very few studies have considered it in a quantitative way. Tools are now available to obtain additional diagnostic information about rock heterogeneity and saturation distribution within a core sample; for instance, imaging techniques such as x-ray Computed Tomography (X-ray CT) [87] or Nuclear Magnetic Resonance Imaging (NMRI) [106, 107] have the potential to dramatically improve the quantitative characterization of reservoir cores at the sub-core (mm/cm) scale [80]. For instance, methodologies have been developed to quantitatively characterize reservoir cores in terms of relevant properties such as the spatial variation of permeability and capillary pressure curves from laboratory displacement tests [86, 88, 108, 109]. Most importantly, the combination of these methods with models that take into account these sub-core scale heterogeneities has been shown to be important for cores with a high degree of heterogeneity [86, 104]. By using information about about the spatial heterogeneity of the core in simulations, it has been shown that it is possible reconsile the "effective" relative permeability of the heterogeneous rock with the "characteristic" relative permeability of a homogeneous subportions of the rock [104]. Moreover, it has been shown that 3 dimensional simulations of the core flood experiments are needed when gravity and capillary forces are significant [105].

5.4. **Problems with Relative Permeability Measurements.**

5.4.1. *Capillary End-Effect.* The most common source of problems encountered in core-flooding tests is the capillary end effect, a phenomenon that results from capillary pressure discontinuities at the inlet and outlet faces of the core. Capillary end effects lead to saturation and capillary pressure gradients along the length of the core that may preclude simple application of Eq. 30 for calculating relative permeability [79]. Among the two end effects, the downstream capillary end seems to be the major concern of most experimentalists and it has been described by Leverett as being the result of *"a discontinuity in the capillary properties of the sand, since the water passes abruptly from a region of relatively high capillary pressure (the sand) into a void in which (since the restraint imposed by the sand grains is absent) the oil-water interface has no sensible curvature, and the capillary pressure therefore vanishes"* [13]. The practical consequence of this phenomenon is that the saturation of the wetting phase at the outflow boundary is maintained at a higher level

than throughout the remainder of the core [90]. This is obviously a problem for those (unsteady) techniques that rely on measurements carried out at the effluent-end and that neglect capillary forces (see above). Additionally, steady-state methods that use the one-dimensional integral form of the extended Darcy's law based on the measurement of the pressure drop across the core are equally affected: in fact, due to the existing saturation gradient, the effective pressure drop across the core causing flow of the wetting phase is less than that causing flow of the non-wetting phase by an amount equal to the difference in capillary pressure at the two ends of the core. If the pressure drop in the wetting phase is assumed to be that in the non-wetting phase, it is evident that the relative permeability to the wetting phase will be underestimated [90]. From an experimental point of view the options two circumvent this problem are therefore two: the end-effect can either be eliminated or it can be accounted for in the analysis of the experimental data by using a suitable mathematical model. In the former case, technical solutions have been proposed that allow for a direct control on the capillary pressure itself (the Hassler apparatus), or where the actual measurement is performed far enough from the inflow and outflow end of the sample, the latter being sandwiched between two samples of similar material (Penn State Method) [90]. Simpler solutions, such as the Single Core Dynamic Method, impose a high displacement rate, as typically the length over which boundary saturation gradients are observed decreases as the injection rate increases [90]. In practice, boundary effects are typically circumvented by using high injection rates. The use of mathematical models with appropriate boundary conditions to explicitly account for capillary effects is another option that should be considered irrespectively of the applied experimental technique [84]. We believe that the success of the latter has been limited by the lack of a proper understanding of the actual outlet boundary condition during a core-flooding experiment. Typically, a zero capillary pressure condition is imposed at the outlet boundary, which has the effect of forcing the nonwetting phase saturation to zero at the outlet and accordingly of setting the relative permeability to the same phase to zero [110]. Physically, this situation might be envisaged as a stream of small droplets of nonwetting phase ("mist") flowing out of the sample, as reported in [111], though for a vertical core-flooding arrangement where a pool of wetting phase was provided at the outlet boundary. Other investigators consider the outlet boundary in more detail. *Richardson aet al.* [112] propose that the capillary pressure at the outlet takes a constant finite value equal to the entry capillary pressure, i.e. the minimum pressure at which the permeability to the nonwetting phase becomes larger than zero, while Heaviside allows for the outlet saturation to change according to Darcy's law [113]. In this context, it is worth pointing out that a better description of the actual boundary condition during core-flooding experiment could be achieved by developing techniques that measure in-situ capillary pressure during a displacement test, such as by using pressure transducers equipped with special wetted membranes [91] or by applying imaging techniques such as x-ray CT scanning [88].

5.4.2. *Capillary pressure limitations.* Very often, experiments carried out with an unfavorable viscosity ratio lead to the observation of *apparent* low end-point values both during unsteady and steady-state core-flooding experiments. As discussed by *Krevor et al.* [23],

this is relevant also to the *sc*CO_2-brine system and it reflects the level of capillary pressure achieved during the core-flood, which in turns is limited by the low viscosity of the injected gas. Unsteady methods based on effluent data are directly limited by the outlet end-effect that precludes achieving higher nonwetting saturations. During a conventional steady-state experiment, the condition is typically not met as the end-point is approached that allows for the application of the integral form of the extended Darcy's law in one dimension. By definition, the achievement of the end-point requires reaching that portion of the capillary pressure curve that rises steeply with saturation. Therefore, despite the presence of capillary end-effects, under these conditions a fairly uniform saturation within the core can be observed. This is however not sufficient, as in a co-injection experiment, the capillary pressure has to be uniform throughout the sample, too. It might be experimentally extremely difficult to meet these conditions without direct control on the capillary pressure itself (as it is the case for the Hassler apparatus [90]). This is shown as an example in Figure 9, where the steady-state saturation and capillary pressure profiles along the length of the core are shown that have been obtained during the *sc*CO_2-brine experiment upon injection CO_2 at 50 mL/min. It can be seen that, indeed, the slice-averaged saturation profile is fairly constant ($S_{\mathrm{w,ave}} = 0.45$), but that this is not true for the capillary pressure (obtained upon application of Eq. (8)), which shows a significant negative and non-linear gradient. In fact, application of the one-dimensional form of the extended Darcy's law for a steady-state experiment, i.e. $k_{\mathrm{r,nw}} = (q_{\mathrm{inj}} L \mu_{\mathrm{nw}})/(Ak\Delta P_{\mathrm{c}})$, results in the underestimation of the CO_2 relative permeability, i.e. $k_{\mathrm{r,nw}}(S_{\mathrm{w,ave}}) \approx 0.4$. However, in the central portion of the core (15-65 mm) the (capillary) pressure gradient is constant ($\Delta P/\Delta x = 34.03$ kPa/mm); application of the same equation leads in this case to $k_{\mathrm{r,nw}}(S_{\mathrm{w,ave}}) \approx 0.94$, thus approaching the absolute permeability of the core.

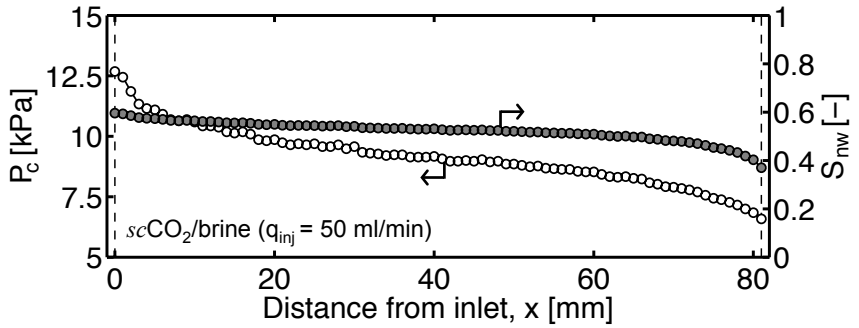

FIGURE 9. Steady-state CO_2 saturation and capillary pressure profiles along the length of a Berea Sandstone core during a *sc*CO_2-brine drainage experiment, as described in [114]. CO_2 is injected 50 mL/min and saturation have been measured by x-ray CT scanning upon achievement of steady-state.

5.5. **Variations on methods for making relative permeability measurements.**

5.5.1. *Multi-Rate Displacement Tests.* Alternative techniques have been proposed to circumvent some of the problems described above and in particular to allow for the measurement of end-point relative permeabilities. In the case of unsteady methods, a so-called multi-rate test is often applied that consists of conduction additional measurements at increasingly higher flow rates after the base displacement test [91]. As already mentioned in the previous sections, excessively high injection rates should always be avoided and their selection should depend on the sample characteristics (permeability, rock's consolidation, etc.). The following non-linear model is then used to fit the apparent endpoint relative permeabilities k_i measured at various flow rates q_i:

$$k_i = a_1 \left(1 - e^{-a_2 q_i}\right) \tag{31}$$

where a_1 and a_2 are the fitting parameters; in particular, the value of the constant a_1 provides an approximation of the true end-point value as the flow rate tends to infinity [Bennion]. Obviously, a new final residual saturation should be determined if additional production of the displaced fluid is monitored.

5.5.2. *Stationary Liquid Method.* The method is applicable only to the determination of relative permeability to the nonwetting phase and was initially proposed by Leas [115] and later adopted by Ramakrishnan and Capiello [116]. This technique was originally developed with the purpose of determining the relative permeability to a gas, as the wetting phase could be held stationary upon application of a very low pressure gradient across the core [115] . The method can be easily extended to other fluid-pairs and higher-pressure gradients (or flow rates), where immobilization of the wetting phase is achieved by achieving steady-state conditions [116]. Its implementation reflects some of the characteristics of a conventional steady-state relative permeability experiment, but it doesn't require the achievement of a uniform saturation within the core, thus allowing generating data up to the endpoint saturation of the nonwetting fluid. In particular, displacement tests are conducted at increasing flow rates and requires the measurement of both fluid saturation at the inlet of the core and the pressure drop across the core. The essential premise for the application of the method is that at steady-state, the wetting phase stops flowing, and the pressure drop measured across the core equals the capillary pressure acting on the inlet face of the core, i.e. $\Delta P = P_1 - P_2 = P_c \mid_{x=0}$. As a matter of fact, a very interesting corollary of the method is that it additionally allows for the measurement of a capillary pressure curve [88]. In fact, with a simultaneous measurement of the saturation at the inlet face of the core (for instance by x-ray CT scanning) the capillary pressure can be directly related to a saturation value, and by repeating the measurement at increasing flow rates, a capillary pressure curve can be constructed [88]. A relative permeability curve can be obtained from the same experimental observations [116, 114]; in particular, the plot of the injection flow rate q_{inj} as a function of the steady-state capillary pressure drop across the core, $\Delta P_c = P_{c,1} - P_{c,2}$, leads to a curve with a slope proportional to the non-wetting phase relative permeability at $x = 0$. Also in this case, the simultaneous measurement of the saturation at the inlet face of the core using the X-Ray CT scanner allows establishing the relation between relative permeability and saturation at that particular position and

pressure drop (or capillary pressure). The following comments are worth making regarding the application of this technique. At high wetting phase relative permeabilities (low flow rates and accordingly small pressure drop), the wetting phase saturation typically reaches a stable value after just a few pore volumes of gas injection. However, as the injection flow rate is increased, the wetting phase saturation is reduced and its relative permeability will decrease, thus requiring the injection many pore volumes to reach a steady-state condition. Additionally, since the method requires to take derivatives of the q_{inj} vs. ΔP_{c} data, usually a curve fit should be applied to reduce the influence of experimental "noise" [116, 114]. Finally, the capillary pressure values at the inlet and outlet ends of the core have to be known; while at $x = 0$ the capillary pressure takes the same value as the measured pressure drop across the core (see above), the outlet boundary condition is not uniquely defined and might depend on the type of system used to perform the experiments. In particular, some studies have assumed a value of zero (as in [116]), while in others impose a constant finite value that is equal to the entry capillary pressure, $P_{\mathrm{c,e}}$, i.e. the minimum pressure at which the permeability to the nonwetting phase takes a finite value, a condition that has to be met within a porous sample and confirmed by experimental observations [112].

6. Existing CO_2 and Brine Relative Permeability Data

In this section, data are presented of relative permeability curves measured with the CO_2/Water system mostly at conditions relevant to the sequestration. When appropriate the data are compared to other fluid-pairs, so as to highlight the major unknowns of the CO_2/Water systems.

6.1. **Relative Permeability.**

Water and CO_2 were chosen as the fluids for the first relative permeability measurement reported on a consolidated sandstone [12]. These early observations have been successively substantiated by several experimental studies that used various fluid-pairs and led to the generalizations that have been described in Section 3. Since those initial measurements, however, little work was performed with the CO_2-brine system and reservoir-condition experiments were not made until CO_2 sequestration development began in the 1990's.

As part of one of the deliverables of the present report, a library of existing relative permeability curves measured with the CO_2-brine system has been created and it can be accessed online [2]; the library includes data from the literature and selected projects suited to both carbonate and sandstone reservoirs. Figure 10 shows the compiled P, T conditions and drainage curves for the published CO_2-brine relative permeability curves in the literature. The great majority of the curves were generated by a single group, with datasets summarized in [59, 117]. The experimental procedure and raw data are reported in [118, 119]. These curves were measured on a wide range of sandstone and carbonate rocks from potential sequestration targets in Canada. For a given experiment, pressure, temperature and brine composition were chosen to match conditions in the reservoir from which the core came. This resulted in the generation of curves across a wide range of pressure, temperature, and salinity conditions. There are few generalizations that can be made from this dataset, and no correlations between relative permeability and other rock properties, e.g. permeability, capillary pressure characteristics, were found [117].

Data from the existing literature leaves a number of questions unresolved for the CO_2-brine system. It is not currently well understood the extent to which reservoir conditions of pressure, temperature and salinity impact the flow properties in a given rock. As discussed in Section 3.3 the literature on this is ambiguous. Some studies have observed variation in the relative permeability within a single rock with changing pressure and temperature conditions or fluid pairs. Decane-brine relative permeability was compared with a $sc CO_2$-brine system in [120] using a Berea sandstone, and it was suggested that the $sc CO_2$-brine system was less strongly water wet. Relative permeability in Berea sandstone across a small range in flow rates and P-T conditions was observed in [121] and was invariant across this range of conditions. Figure 11 shows the CO_2 relative permeability data measured by *Botset* [12] (on a Nichols buff sandstone), together with results from other studies that used Berea

[2] https://pangea.stanford.edu/research/bensonlab/relperm/.

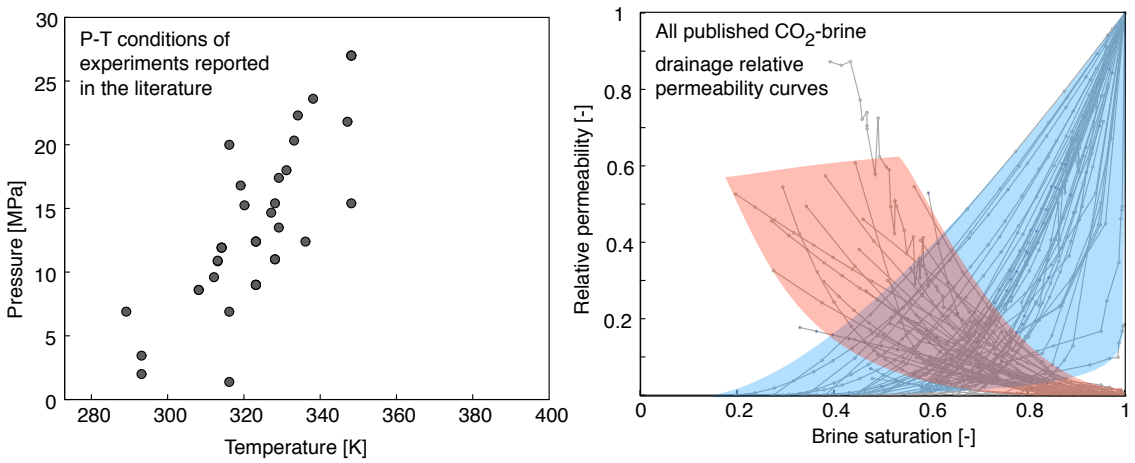

FIGURE 10. Left: Pressure and temperature conditions of all of the drainage CO_2-brine relative permeability measurements reported in the literature. Note many experiments were performed at repeat conditions, with different rock samples. Right: All of the relative permeability curves superimposed onto one plot. The data is compiled from [34, 59, 117, 12, 120, 23, 121].

Sandstone cores and various gas/liquid pairs, thus including recent data with the *sc*CO_2-brine system. Additional details about fluids, rock and applied experimental conditions are summarized in Table 3. Given the wide range of permeability (100-1000mD) and the variety of fluid pairs involved, it is safe to conclude that the different studies on Berea Sandstone yield a similar drainage relative permeability curve, though discrepancies are noticed for the brine relative permeability data reported in [34]. In the latter case, a different experimental procedure was adopted as compared to the conventional approach (see Section 5.2), as at each fractional flow, the total flow rate was varied in order to maintain a relatively constant capillary number during the course of the experiment. In general, however, this dataset on Berea Sandstone cores would suggest that within the precision of the measurements, relative permeability for the *sc*CO_2-brine system is not substantially different than other fluid pairs in water-wet rocks; in fact the relative permeability data have been obtained from two different laboratories in three independent studies that have been measured for the *sc*CO_2-brine-Berea Sandstone system upon application of the steady-state core-flooding technique (see caption for more details) and shows that general agreement can be also obtained between independent laboratories.

For *sc*CO_2 there are no relative permeability measurements at high saturations and permeabilities usually associated with a non-wetting phase. For all of the *sc*CO_2-brine experiments it can be seen from Figure 10 that observed maximum gas saturations are generally less than 0.5 and the measured relative permeabilities are low ($k_{\mathrm{r,nw}} < 0.2$). Very similar

TABLE 3. Studies reporting relative permeability measurements on Berea Sandstone cores and various gas/liquid fluid pairs. [a] From *Yan et al.* [122]. [b] Based on the total molality of the solution from data reported in *Li et al.* [56]. [c] From *Chun and Wilkinson* [123]. [d] Based on the viscosity of an aqueous NaCl solution from data reported in *Kestin and Shankland* [124]. [e] NIST chemistry web book (http://webbook.nist.gov).

Reference	Fluids	T/P [°C]/[MPa]	k [mD]	D/L [cm]/[cm]	γ_{12} [mN/m]	μ_w/μ_{nw}
**Botset* [12]	gCO$_2$/Water	-	500	10.2/136.6	-	-
Richardson aet al. [112]	He/Kerosene	-	118	1.85/7.23	-	-
Brooks and Corey [15]	Air/Hydrocarbon liq.	-	348	- / -	-	-
Oak et al. [14]	N$_2$-brine (1.5 mol/kg)	21/5.5	185	5.1/7.6	70[a]	56[d,e]
?]	scCO$_2$-brine (0.13 mol/kg)	50/12.4	430	5.08/15.24	34[b]	12[e]
Krevor et al. [23]	scCO$_2$/Water	50/9.0	914	5.0/10.0	37[b]	24[e]
Akbarabadi and Piri [34]	scCO$_2$-brine (1.6 mol/kg)	55/11.0	612	3.76/15.4	38[b]	56[d,e]

*On a Nichols buff sandstone.

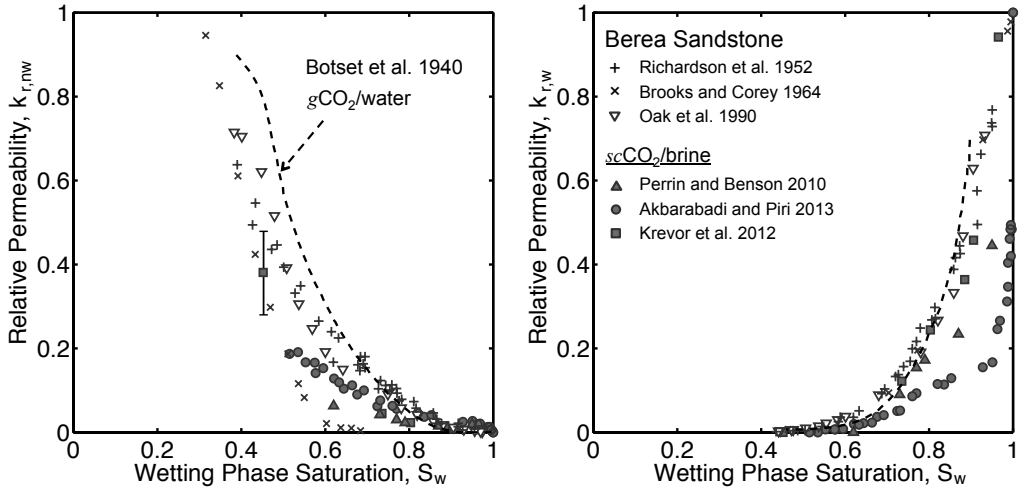

FIGURE 11. Drainage relative permeability curves measured on Berea Sandstone cores with various gas-liquid fluid pairs. Symbols are data taken from the literature (details are given in Table 3). Note that results by *Botset* [12] (dashed line) were obtained with CO_2 and water on a Nichols Buff sandstone and they represent the first relative permeability measurements reported on a consolidated rock.

results are reported by *Bachu and Bennion* [59] for CO_2-brine relative permeability curves measured on numerous sandstone and carbonate samples, together with the observation of a particularly strong effect of the interfacial tension on the shape of the relative permeability curves across the range of 20 to 56 mN/m. While the low end-points values have been attributed to rock heterogeneity (channeling and bypassing) [59, 125], the sensitivity to interfacial tension suggests that the comparison of the scCO$_2$-brine system with other

(more conventional) gas-liquid pairs (such as N_2-brine) is not straightforward [125]. However, the dataset shown in Figure 11 that include various studies using similar rock samples but different fluid-pairs doesn't substantiate some of these arguments. Similarly the level of rock heterogeneity was found to have no impact on this property in [23]. *Krevor et al.* [23] explains that *apparent* low end-point values are the result of the maximum capillary pressure achievable during the core-flood. Due to the low viscosity of CO_2, it is difficult to acheive high saturations in the core in the presence of a capillary end effect [126]. Achieving high saturations requires extremely large pressure gradients across the core, which can only be obtained at flow rates that might be experimentally inaccessible or for very long cores. It is notable that the singular exception to the low apparent endpoint in Figure 10 is from the experiments of *Botset* [12], which were performed on cores greater than 1m in length in which much higher capillary pressures may be achieved. Nevertheless, the observation of measured low end-point relative permeabilties and high irreducible saturations remain and open question requiring further study, and indeed are expected for capillary dominated conditions in highly heterogenous rocks [104].

6.2. **Imbibition and Trapping Curves.** Beside the measurement of capillary pressure and relative permeability curves for the *sc*CO_2-brine system, experiments are just beginning that aim at characterizing and quantifying the hysteretic behavior of these properties. An example of drainage-imbibition relative permeability curves for the *sc*CO_2-brine measured on a Berea Sandstone core [34] is shown in Figure 12 and it is compared to experimental results obtained for an Oil/Water system [14]. In the latter case, the observations are in agreement with the general trend observed for systems characterized by a strong wettability, where the nonwetting phase tends to have a lower permeability during imbibition than it does during drainage, while the wetting phase relative permeability values typically retrace those obtained during drainage [16]. In other words, under such conditions, the relative permeability to the wetting phase can be assumed to be a function only of its own saturation. Interestingly, the *sc*CO_2-brine-Berea Sandstone system seems to behave differently, with the relative permeability to both phases being affected by the direction of the saturation change. Whether this behavior is caused by a different wetting character of this system or by a peculiarity of the *sc*CO_2-brine requires more experimental work under a variety of conditions and rock types.

Typically, the trapping characteristics of a given fluid-pair system are summarized through the so-called initial-residual (IR) curve, where the maximum (initial) nonwetting phase saturation is plotted as a function of its residual saturation [4]. Figure 13 shows IR data for *sc*CO_2 and Brine on Berea Sandstone as obtained from three different laboratory studies. In the figure, the data are compared to the Land model [30], a correlation used to predict trapped gas saturations that is commonly applied in the petroleum industry (see also Section 2.3). It can be seen that the agreement among the three sets of data is satisfactory and that the same is true for the match between experiments and model. Most importantly, the results provide direct experimental evidence that residual trapping can immobilize a large fraction of injected CO_2 (up to 40% for initial saturation ranging between 60 and

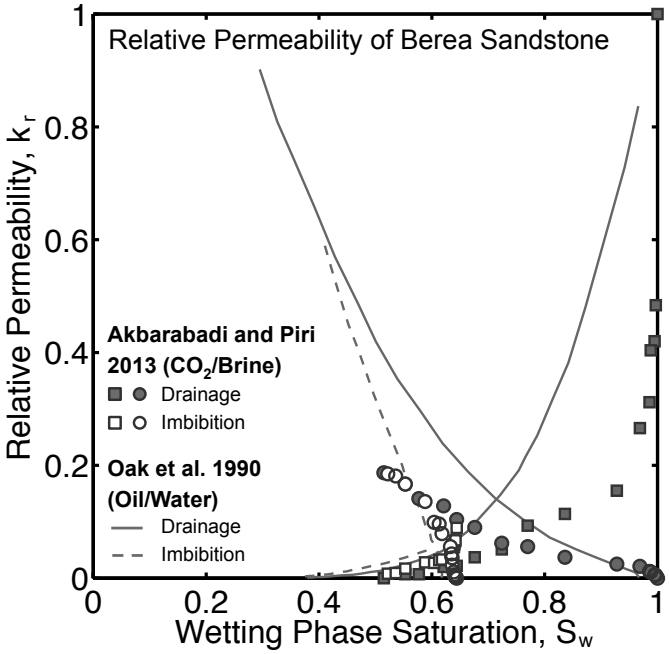

FIGURE 12. Drainage-Imbibition relative permeability curves of Berea Sandstone for the $sc\mathrm{CO}_2$-brine [34] and Oil/Water [14] systems. The following experimental conditions apply: *Akbarabadi and Piri 2013*, P=11 MPa, T=55°C, permeability k=612 mD, brine molality 1.6 mol/kg [34]; *Oak et al. 1990*, P=5.5 MPa, T=21°C, permeability k=185 mD, brine molality 1.5 mol/kg [14].

80%). For the sake of comparison, trapped gas saturation between 23 and 69% from an initial gas saturation of about 80% have been reported for gas/liquid displacement experiments in carbonate reservoir rocks [127], while lower values (ranging from 10% to 30%) were observed during experiments with CO_2 and brine in low permeability sandstones [59].

It is worth pointing out that if the dataset for relative permeability measurements with $sc\mathrm{CO}_2$ and water is scarce, the experimental characterization of imbibition curves is almost nonexistent. This makes the evaluation of the theories and concepts just described more difficult, in particular when considering the use of analog fluids and experimental conditions to characterize petrophysical properties useful in modeling subsurface $sc\mathrm{CO}_2$/water systems [23]. With relevance to the hysteretic character of the relative permeability curve, it has been occasionally observed that a small portion of the drainage curve is retraced before a unique imbibition curve can be identified [128, 33]. Interestingly enough, this behavior has been observed in a recent study during $sc\mathrm{CO}_2$/water core-flooding experiments on a Berea Sandstone [34]. The reason for this phenomenon might be traced back to the particular

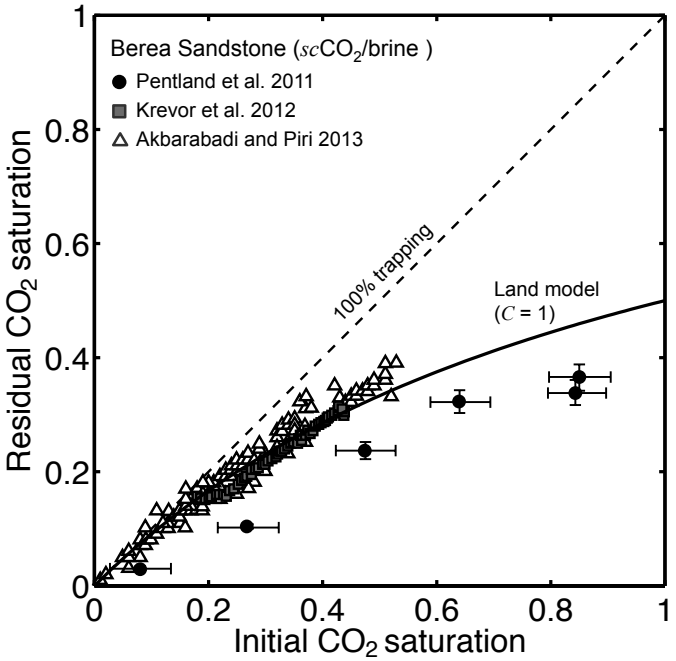

FIGURE 13. Initial-Residual (IR) curve for the $sc\mathrm{CO}_2$-brine system on Berea Sandstone; data are compared from three different studies, namely *Pentland et al. 2011* (P=9 MPa, T=70°C, permeability, k=460 mD, brine molality 0.82 mol/kg [22], *Krevor et al. 2012*, P=9 MPa, T=50°C, permeability k=914 mD, fresh water [23], *Akbarabadi and Piri 2013*, P=11 MPa, T=55°C, permeability k=612 mD, brine molality 1.6 mol/kg [34]. The solid line represent a prediction using the Land model with a trapping coefficient C=1.

geometry and topology of the pore space, as studies on glass micro models have shown that a small pore-to-throat ratio might lead to a dynamics of multiphase flow that are completely reversible [129]. Regardless of the actual mechanism, this example highlights once more the need for more experimental observations of the CO_2/water systems at conditions relevant to geologic carbon sequestration, as this phenomenon would significantly affect the amount of CO_2 that can be immobilized by residual trapping within a storage formation and eventually play a large role in the long term security of a storage project.

7. Gaps and Data Needs for Establishing Reliable Relative Permeability Relationships for CO_2 Storage

Relative permeability curves during both drainage and imbibition are a key determinant of the fate and transport of CO_2 over the lifetime of a storage project. To date only limited information on these critical parameters is available. Many open questions remain about the proper values to use, the most reliable measurement techniques, whether analogue fluids/conditions can be reliably used for making measurements and how to deal with the heterogeneities present in reservoir rocks. While the concept of relative permeability is well established and reliable datasets are available for the oil-water system, the CO_2-brine system poses unique challenges that require special consideration. Specifically, the very low viscosity of CO_2 compared to water, creates a system where viscous forces are much smaller than the oil-water system and tend to be more capillary dominated. This affects both the ability to make reliable relative permeability measurements as well as potentially increasing the importance of the fluid properties on multiphase flow behavior. The following summarizes major gaps and makes recommendations for a set of experiments to resolve them.

1. Influence of interfacial tension, wettability and viscosity on drainage relative permeability in CO_2-brine Systems. Data in the literature provide contradictory conclusions about the role of interfacial tension and viscosity on the relative permeability curves. We recommend carrying out a set of relative permeability experiments that definitively demonstrate and quantify the role of variations of these parameters on the CO_2-brine relative permeability curves. It is important to ensure the that effects of viscosity, wettability and interfacial tension are individually assessed. Careful selection of the pressure and temperature conditions are needed to accomplish this.

2. Comparison of methods for making relative permeability measurements. A systematic comparison of methods for making CO_2 brine measurements has not been undertaken. The wide range of relative permeability curves, the low end-point relative permeability to CO_2 and high irreducible water saturations suggests that some of the varaibility between data sets can be explained by the different methods used to measure them. We recommend making a set of measurements using a variety of techniques on a number of representative rock cores in order to establish the aggreement or lack thereof between different measurement techniques.

3. Investigation of the low end-point relative permeabilities and high irreducible water saturations. Most of the existing data sets suggest that the end-point relative permeability to CO_2 is low (<0.5) and that the residual water saturation is high ($S_{wir} > 0.4$). On the other hand, theoretical considerations and limitations of experimental techniques suggest that this may be an artifact of the measurement techniques. We recommend a systematic study to explain these observations. Important variables include flow rates, degree of heterogeneity of the core, and experimental design.

4. Development of a larger data set for imbibition relative permeability curves. Very little information is available for the CO_2-brine system about hysterisis and the extent of residual gas trapping, and how it depends on fluid properties, imbibition rates, and rock heterogeneity. There is a great need for more core-scale imbibition relative permeability measurements. We recommend conducting a systematic study of imbibition relative curves over the typical range of conditions (pressure, temperature and brine salinity) and for a relevant set of reservoir rocks to fill this gap.

5. Identification of best practices for making relative permeability measurements for CO_2-brine systems. Today, relative permeability measurements have been made using a number of different methods, including steady state, transient, and stationary fluid methods. Given the unique properties of the CO_2-brine system, resulting from low viscosity of CO_2 relative to brine and high interfacial tension, there is need to develop best practices for making relative permeabilty measurements for CO_2 storage projects. We recommend that based on an assessment of the above issues, standard protocols for making relative permeabilty measurements for the CO_2-brine system be developed.

References

[1] Bear, J. *Dynamics of Fluids in Porous Media* Academic Press, San Diego, 1992

[2] Dullien, F.A.L. *Porous Media Fluid Transport and Pore Structure* American Elsevier Publishing Company, New York, 1972

[3] Lake, L.W. *Enhanced Oil Recovery* Society of Petroleum Engineers, Richardson, Texas 1989

[4] Lake., L.W. *Enhanced Oil Recovery.* Prentice Hall, 1996.

[5] Hubbert, M. K. The Theory of Ground-Water Motion *The Journal of Geology*, 48(8)1:785-944, 1940

[6] Wyckoff, R.D., and H.G. Botset The Flow of Gas Liquid Mixtures Through Unconsolidated Sands, *Physics*, 7(9):325-345, 1936

[7] Muskat, M., and M.W. Meres The Flow of Heterogeneous Fluids Through Porous Media, *Physics*, 7(9):346-363, 1936

[8] Muskat, M. *Physical Principles of Oil Production* McGraw-Hill Book Co., 1949

[9] Avraam, D.G. and A.C. Payatakes Flow regimes and relative permeabilities during steady-state two-phase flow in porous media *Journal of Fluid Mechanics*, 293:207-236, 1995

[10] Kovscek, A.R., H. Wong, C.J. Radke A Pore-Level Scenario for the Development of Mixed Wettability in Oil Reservoirs *Environmental and Energy Engineering*, 39(6):1072-1085, 1993

[11] Amyx, J.W., D.M. Bass, and R.L. Whiting. *Petroleum reservoir engineering. Physical properties.* McGraw-Hill Book Company, Inc., 1988.

[12] Botset, H.G. Flow of gas-liquid mixtures through consolidated sand. *Transactions of the AIME*, 136(1):91–105, 1940.

[13] Leverett, M.C., Flow of oil-water mixtures through unconsolidated sands. *Transactions of the AIME*, 132(1):149–171, 1939.

[14] Oak, M.J., L.E. Baker, and D.C. Thomas. Three-phase relative permeability of Berea Sandstone. *Journal of Petroleum Technology*, 42(8):1054–1061, 1990.

[15] Brooks, R.H., and A. T. Corey. Hydraulic properties of porous media. *Hydrology Paper No. 3, Colorado State University*, 3:1–27, 1964.

[16] Craig, F.F. *The Reservoir Engineering Aspects of Waterflooding.* SPE Monograph Series 3, Society of Petroleum Engineers., 1971.

[17] Morgan, J.T., and D.T. Gordon. Influence of pore geometry on water-oil relative permeability. *Journal of Petroleum Technology*, 22(10):1199–1208, 1970.

[18] Kim, Y., J. Wan, T.J. Kneafsey, and T.K. Tokunaga. Dewetting of silica surfaces upon reactions with supercritical CO_2 and brine: pore-scale studies in micromodels. *Environmental Science and Technology*, 46(7):4228–4235, 2012.

[19] Lenormand, R., C. Zarcone, and A. Sarr. Mechanisms of the displacement of one fluid by another in a network of capillary ducts. *Journal of Fluid Mechanics*, 135:337–353, 1983.

[20] Juanes, R., E.J. Spiteri, F.M. Orr Jr., and M.J. Blunt. Impact of relative permeability hysteresis on geological CO_2 storage. *Water Resources Research Res.*, 42:1–13, 2006.

[21] Hovorka, S.D., S.M. Benson, C. Doughty, B. M. Freifeld, S. Sakurai, T. M. Daley, Y. K. Kharaka, M. H. Holtz, R. C. Trautz, H. S. Nance, L. R. Myer, and K. G. Knauss. Measuring permanence of CO_2 storage in saline formations: the Frio experiment. *Environmental Geosciences*, 13(2):105–121, 2006.

[22] Pentland, C.H., R. El-Maghraby, S. Iglauer, and M. J. Blunt. Measurements of the capillary trapping of super-critical carbon dioxide in Berea sandstone. *Geophysical Research Letters*, 38:L06401, 2011.

[23] Krevor, S.C.M., R. Pini, L. Zuo, and S. M. Benson. Relative permeability and trapping of CO_2 and water in sandstone rocks at reservoir conditions. *Water Resources Research*, 48(2):W02532, 2012.

[24] Genuchten. M.T.V A closed-form equation for predicting the hydraulic conductivity of unsaturated soils1. *Soil Science Society of America journal*, 44(5):892–898, 1980.

[25] Purcell, W.R., Capillary pressures-their measurement using mercury and the calculation of permeability therefrom. *Journal of Petroleum Technology*, 1(2):39–48, 1949.

[26] Gates, J.I. and W.T. Lietz. Relative permeabilities of California cores by the capillary-pressure method. *Drilling and Production Practice*, API Conference Paper:285–302, 1950.

[27] Burdine, N.T. Relative permeability calculations from pore size distribution data. *Journal of Petroleum Technology*, 5(3):71–78, 1953.

[28] Burdine, N.T., L.S. Gournay, and P.P. Reichertz. Pore size distribution of petroleum reservoir rocks. *Journal of Petroleum Technology*, 2(7):195–204, 1950.

[29] Mualem, Y. Hysteretical models for prediction of the hydraulic conductivity of unsaturated porous media. *Water Resources Research*, 12(6):1248–1254, 1976.

[30] Land, C.S. Calculation of imbibition relative permeability for two- and three-phase flow from rock properties. *SPE Journal*, 8(2):149–156, 1968.

[31] Spiteri, E., R. Juanes, M. Blunt, and F. Orr. A new model of trapping and relative permeability hysteresis for all wettability characteristics. *SPE Journal*, 13(3):277–288, 2008.

[32] Krevor, S.C.M., R. Pini, B. Li, and S.M. Benson. Capillary heterogeneity trapping of CO_2 in a sandstone rock at reservoir conditions. *Geophysical Research Letters*, 38:L15401, 2011.

[33] Carlson, F. Simulation of relative permeability hysteresis to the nonwetting phase. In *56th Annual Fall Technical Conference and Exhibition of the Society of Petroleum Engineers of AIME, San Antonio, Texas (USA), October 5-7*, 1981.

[34] Akbarabadi, M., and M. Piri. Relative permeability hysteresis and capillary trapping characteristics of supercritical CO_2/brine systems: An experimental study at reservoir conditions. *Advances in Water Resources*, 52(0):190–206, 2013.

[35] Killough, J.E. Reservoir simulation with history-dependent saturation functions. *SPE Journal*, 16(1):37–48, 1976.

[36] Muskat, M. The flow of fluids through porous media. *Journal of Applied Physics*, 8(4):274–282, 1937.

[37] Reeves, P.C., and M.A. Celia A functional relationship between capillary pressure, saturation, and interfacial area as revealed by a pore-scale network model *Water Resources Research*, 32(8):2345-2358, 1996

[38] Joekar-Niasar, V., S.M. Hassanizadeh, A. Leijnse Insights into the Relationships Among Capillary Pressure, Saturation, Interfacial Area and Relative Permeability Using Pore-Network Modeling *Transport in Porous Media* 74:201-219, 2008

[39] Buckley, S.E., and M.C. Leverett Mechanism of Fluid Displacement in Sands *Transactions of the AIME*, 146(1):107-116, 1942

[40] O'Meara Jr., D. J. and W. O. Lease. Multiphase relative permeability measurements using an automated centrifuge. In *SPE 58th Annual Technical Conference and Exhibition, San Francisco, California (USA), October 5-8*, 1983.

[41] Honarpour, M. M., Koederitz L., and Harvey A. H., Relative Permeability of Petroleum Reservoirs. *CRC Press Ltd.*, 1986.

[42] Perrin, J.-C., K. M. Krause, C.-W. Kuo, L. Miljkovic, E. Charoba, and S. M. Benson. Core-scale experimental study of relative permeability properties of CO_2 and brine in reservoir rocks. *Energy Procedia*, 1(1):3515–3522, 2009.

[43] Bachu, S. Screening and ranking of sedimentary basins for sequestration of CO_2 in geological media in response to climate change *Environmental Geology*, 44:277-289, 2003

[44] Nordbotten, J. M., M. A. Celia, and S. Bachu. Injection and storage of CO_2 in deep saline aquifers: Analytical solution for co 2 plume evolution during injection. *Transport in Porous Media*, 58(3):339–360, 2005.

[45] Hanor, J.S. Origin of saline fluids in sedimentary basins. In: Geofluids: Origin, Migration and Evolution of Fluids in Sedimentary Basins (ed J. Parnell), *Geological Society of London Special Publication*, 78:151-174, 1994

[46] Phillips, S.L., A. Igbene, J.A. Fair, H. Ozbek, M. Tazana A Technical Databook for Geothermal Energy Utilization. *Lawrence Berkeley Laboratory Report* 12810

[47] Span, R, and W. Wagner A New Equation of State for Carbon Dioxide Covering the Fluid Region from the Triple-Point Temperature to 1100K at Pressures up to 800 MPa *The Journal of Physical and Chemical Reference Data*, 25(6): 1509-1596, 1996

[48] Kestin, J., H. E. Khalifa, and R. J. Correia Tables of the Dynamic and Kinematic Viscosity of Aqueous NaCl Solutions in the Temperature Range 50-150 °C and the Pressure Range 0.1-35 MPa *The Journal of Physical and Chemical Reference Data*, 10(1):71-87,1981

[49] Fenghour, A., W.A. Wakeham, V. Vesovic The Viscosity of Carbon Dioxide *The Journal of Physical and Chemical Reference Data*, 27(1):31-44, 1998

[50] Duan, Z., and R. Sun An improved model calculating CO_2 solubility in pure water and aqueous NaCl solutions from 273 to 533 K and from 0 to 2000 bar *Chemical Geology*, 193:257-271, 2003

[51] Duan, Z., R. Sun, C. Zhu, I-M. Chou An improved model calculating CO_2 solubility in aqueous solutions containing Na^+, K^+, Ca^{2+}, Mg^{2+}, Cl^-, and SO_4^{2-} *Marine Chemistry*, 193:257-271, 2006

[52] Chiquet, P., J-L. Daridon, D. Broseta, S. Thibeau CO_2/water interfacial tensions under pressure and temperature conditions of CO_2 geological storage *Energy Conversion and Management*, 48:736-744, 2006

[53] Bachu, S., and D.B. Bennion Interfacial Tension between CO_2, Freshwater, and Brine in the Range of Pressure (2 to 27) MPa, Temperature from (20 to 125)°C, and Water Salinity from (0 to 334 000) mg·L^{-1} *Journal of Chemical Engineering Data*, 54:765-775, 2009

[54] Chalbaud, C., M. Robin, J-M. Lombard, F. Martin, P. Egermann, H. Bertin Interfacial tension measurements and wettability evaluation for geological CO_2 storage *Advances in Water Resources*, 32:98-109, 2009

[55] Espinoza, D.N., and J.C. Santamarina Water-CO_2-mineral systems: Interfacial tension, contact angle, and diffusion-Implications to CO_2 geological storage *Water Resources Research*, 46:W07537, 2010

[56] Li, X., E.S. Boek, G.C. Maitland, J.P.M. Trusler Interfacial Tension of (Brines + CO_2): $CaCl_2$ (aq), $MgCl_2$(aq), and Na_2SO_4(aq) at Temperatures between (343 and 423) K, Pressure between (2 and 50 MPa), and Molalities of (0.5 to 5) mol·kg^{-1} *Journal of Chemical and Engineering Data*, 57:1369-1375, 2012

[57] Kim, Y., J. Wan, T.J. Kneafsey, T.K. Tokunaga Dewetting of Silica Surfaces upon Reactions with Supercritical CO_2 and Brine: Pore-Scale Studies in Micromodels *Environmental Science and Technology*, 46 (7):4228-4235, 2012

[58] Jung, J-W., and J. Wan Supercritical CO_2 and Ionic Strength Effects on Wettability of Silica Surfaces: Equilbrium Contact Angle Measurements *Energy & Fuels*, 26:6053-6059, 2012

[59] Bachu, S. and B. Bennion., Effects of in-situ conditions on relative permeability characteristics of CO_2-brine systems. *Environmental Geology*, 54(8):1707–1722, 2008.

[60] Fulcher Jr., R. A., T. Ertekin, and C. D. Stahl. Effect of Capillary Number and Its Constituents on Two-Phase Relative Permeability Curves. *Journal of Petroleum Technology*, 37(2):249–260, 1985.

[61] Amaefule, J. O. and L. L. Handy. The Effect of Interfacial Tensions on Relative Oil/Water Permeabilities of Consolidated Porous Media. *Old SPE Journal*, 22(3):371–381, 1982.

[62] Bardon, C. and D. G. Longeron. Influence of Very Low Interfacial Tensions on Relative Permeability. *Old SPE Journal*, 20(5):391–401, 1980.

[63] Yuster, S. T., Theoretical considerations of multiphase flow in idealized capillary systems. *Proceedings of the 3rd World Petroleum Congress*, 2: 437–445, 1951.

[64] Odeh, A. S. The Effect of Viscosity Ratio on Relative Permeability. *Trans., AIME*, 216:346-353, 1959.

[65] Ehrlich, R., Viscous Coupling in Two-Phase Flow in Porous Media and Its Effect on Relative Permeabilities. *Transport in Porous Media*, 11(3): 201–218, 1993.

[66] Lefebvre du Prey, E. J. Factors Affecting Liquid-Liquid Relative Permeabilities of a Consolidated Porous Medium. *Old SPE Journal*, 13(1):39–47, 1973.

[67] Downie, J. and F. E. Crane. Effect of Viscosity on Relative Permeability. *Old SPE Journal*, 1(2):59–60, 1961.

[68] Adams, J. J. and S. Bachu. Equations of state for basin geofluids: algorithm review and intercomparison for brines. *Geofluids*, 2:257–271, 2002.

[69] Mungan, N., Interfacial Effects in Immiscible Liquid-Liquid Displacement in Porous Media. *Old SPE Journal*, 6(3): 247–253, 1966.

[70] Batycky, J. and McCaffery, F., *Low interfacial tension displacement studies*. Petroleum Society of Canada Annual Technical Meeting, 1978

[71] Bennion, D. B. and Bachu, S., Drainage and Imbibition Relative Permeability Relationships for Supercritical CO_2/Brine and H_2S/Brine Systems in Intergranular Sandstone, Carbonate, Shale, and Anhydrite Rocks. *SPE Reservoir Evaluation and Engineering*, 11(3): 487–496, 2008.

[72] Bennion, B. and S. Bachu. The Impact of Interfacial Tension and Pore-Size Distribution/Capillary Pressure Character on CO_2 Relative Permeability at Reservoir Conditions in CO_2-Brine Systems. *SPE/DOE Symposium on Improved Oil Recovery*, pages 1–10, January 2006.

[73] Bennion, D. and Bachu, S., Dependence on temperature, pressure, and salinity of the IFT and relative permeability displacement characteristics of CO_2 injected in deep saline aquifers. *In: SPE 102138, proceedings of the SPE annual technical conference and exhibition, San Antonio, Texas*, 2427 September, 2006.

[74] Moore, T. F. and R. L. Slobod. Displacement of Oil by Water-Effect of Wettability, Rate, and Viscosity on Recovery. *Fall Meeting of the Petroleum Branch of AIME*, pages 1–16, 1955.

[75] Anderson, W.G. Wettability literature survey - Part 4: Effects of wettability on capillary pressure. *Journal of Petroleum Technology*, 39(10):1283–1300, 1987.

[76] Land, C., Comparison of calculated with experimental imbibition relative permeability. *Old SPE Journal*, 11(4): 419–425, 1971.

[77] Aziz, K. and A. Settari *Petroleum Reservoir Simulation* Applied Science Publishers LTD, London, 1979

[78] Honarpour, M., N. Djabbarah, and K. Sampath. Whole core analysis-experience and challenges. *SPE Reservoir Evaluation & Engineering*, 8(6):460–469, 2005.

[79] Honarpour, M. and S.M. Mahmood. Relative-permeability measurements: An overview. *Journal of Petroleum Technology*, 40(8):963–966, 1988.

[80] Heaviside, J. and H. J. Salt. A systematic approach: the key to successful core analysis. In *SPE European Petroleum Conference, London (UK), October 16-19*, pages 463–473, 1988.

[81] Zhou, D., F. J. Fayers, and F. M. Orr. Scaling of multiphase flow in simple heterogeneous porous media. *SPE Reservoir Engineering*, 12(3):173–178, 1997.

[82] Blunt, M. and P. King. Macroscopic parameters from simulations of pore scale flow. *Physical Review A*, 42(8):4780–4787, 1990.

[83] Kopp, A., H. Class, and R. Helmig. Investigations on CO_2 storage capacity in saline aquifers part 1. dimensional analysis of flow processes and reservoir characteristics. *International Journal of Greenhouse Gas Control*, 3:263–276, 2009.

[84] Batycky, JP, FG McCaffery, PK Hodgins, and DB Fisher. Interpreting relative permeability and wettability from unsteady-state displacement measurements. *SPE Journal*, 21(3):296–308, 1981.

[85] Hilfer, R., and P. E. Oren. Dimensional analysis of pore scale and field scale immiscible displacement. *Transport in Porous Media*, 22:53–72, 1996.

[86] Krause, M.H. Modeling and investigation of the influence of capillary heterogeneity on relative permeability. In *SPE Annual Technical Conference and Exhibition, San Antonio, Texas (USA), October 8-10*, 2012.

[87] Akin, S. and A. R. Kovscek. Computed tomography in petroleum engineering research. In F. Mees, R. Swennen, M. Van Geet, and P. Jacobs, editors, *Applications of X-ray Computed Tomography in the Geosciences*, volume 215, pages 23–38. Geological Society, London, 2003.

[88] Pini, R., S. C. M. Krevor, and S. M. Benson. Capillary pressure and heterogeneity for the CO_2/water system in sandstone rocks at reservoir conditions. *Advances in Water Resources*, 38:48–59, 2012.

[89] Morse, R.A., P.L. Terwilliger, S.T. Yuster Relative permeability measurements on small core samples *Oil and Gas Journal*, 46 (109) 1947.

[90] Osoba, J.S., J.G. Richardson, J.K. Kerver, J.A. Hafford, and P.M. Blair. Laboratory measurements of relative permeability. *Journal of Petroleum Technology*, 3(5):47–56, 1951.

[91] Bennion, D.B., and F. B. Thomas. Recent improvements in experimental and analytical techniques for the determination of relative permeability data from unsteady state flow experiments. In *SPE 10th Technical Conference and Exposition, Port of Spain, Trinidad, 26-28 June*, 1991.

[92] Christiansen, R.L., J. S. Kalbus, and S. M. Howarth. Evaluation of methods for measuring relative permeability of anhydrite from the salado formation: Sensitivity analysis and data reduction. Sand94-1346, Sandia National Laboratories, 1997.

[93] Slobod, R.L., A. Chambers, and W. L. Prehn Jr. Use of centrifuge for determining connate water, residual oil, and capillary pressure curves of small core samples. *Petroleum Transactions (AIME)*, 192:127–134, 1951.

[94] Hagoort, J. Oil recovery by gravity drainage. *SPE Journal*, 20(3):139–150, 1980.

[95] Welge, H.J. A simplified method for computing oil recovery by gas or water drive. *Petroleum Transactions (AIME)*, 195:91–98, 1952.

[96] Johnson, E.G., D. P. Bossler, and V. O. Naumann. Calculation of relative permeability from displacement experiments. *Petroleum Transactions (AIME)*, 216:370–372, 1959.

[97] Richmond, P.C. and AT Watsons. Estimation of multiphase flow functions from displacement experiments. *SPE Reservoir Engineering*, 5(1):121–127, 1990.

[98] Archer, J. and SW Wong. Use of a reservoir simulator to interpret laboratory waterflood data. *SPE Journal*, 13(6):343–347, 1973.

[99] Sigmund, P.M. and FG McCaffery. An improved unsteady-state procedure for determining the relative-permeability characteristics of heterogeneous porous media (includes associated papers 8028 and 8777). *SPE Journal*, 19(1):15–28, 1979.

[100] MacMillan, D.J. Automatic history matching of laboratory corefloods to obtain relative-permeability curves. *SPE Reservoir Engineering*, 2(1):85–91, 1987.

[101] Firoozabadi A. and K. Aziz. Relative permeability from centrifuge data. In *56th California Regional Meeting of the Society of Petroleum Engineers, Oakland, California (USA), April 2-4*, 1986.

[102] Hirasaki, GJ , JA Rohan, and JW Dudley. Modifications of centrifuge and software for determination of relative permeability curves. *SPE 25290*, 1992.

[103] Kerig, P. D. and A. T. Watson. Relative-permeability estimation from displacement experiments: An error analysis. *SPE Reservoir Engineering*, 1(2):175–182, 1986.

[104] Krause, M., S.C. Krevor, and S.M. Benson, 2013. A Procedure for the Accurate Determination of Sub-Core Scale Permeability Distributions with Error Quantification. In *Transport in Porous Media*, in press.

[105] Kuo, C-W., J-C Perrin, and S M. Benson, Effect of Gravity, Flow Rate, and Small Scale Heterogeneity on Multiphase Flow of CO2 and Brine In *SPE 132607, Western North America Regional Meeting held in Anaheim*, California, USA, 2630 May 2010.

[106] Chen, S. , F. Qin, K. H. Kim, and A. T. Watson. Nmr imaging of multiphase flow in porous media. *AIChE journal*, 39(6):925–934, 1993.

[107] Davies, S. , A. Hardwick, K. Spowage, and KJ Packer. Fluid velocity imaging of reservoir core samples. *Magnetic resonance imaging*, 12(2):265–268, 1994.

[108] Krause, M.H., Perrin, J-C., and S. M. Benson. Modeling permeability distributions in a sandstone core for history matching coreflood experiments. *SPE Journal*, (12):768–777, 2011.

[109] Shi, J-Q., Z. Xue, and S. Durucan. Supercritical CO_2 core flooding and imbibition in Tako sandstone-influence of sub-core scale heterogeneity. *International Journal of Greenhouse Gas Control*, 5(1):75–87, 2011.

[110] Huang, D. D., and M. M. Honarpour. Capillary end effects in coreflood calculations. *Journal of Petroleum Science and Engineering*, 19(1):103–117, 1998.

[111] Fordham, EJ , LD Hall, TS Ramakrishnan, MR Sharpe, and C. Hall. Saturation gradients in drainage of porous media: Nmr imaging measurements. *AIChE journal*, 39(9):1431–1443, 1993.

[112] Richardson,JG , JK Kerver, JA Hafford, and JS Osoba. Laboratory determination of relative permeability. *Journal of Petroleum Technology*, 4(8):187–196, 1952.

[113] Heaviside,J. , and CJJ Black. Fundamentals of relative permeability: experimental and theoretical considerations. In *SPE 58th Annual Technical Conference and Exhibition held, San Francisco, CA (USA), October 5-8*, 1983.

[114] Pini, R. and S. M. Benson. Simultaneous measurement of capillary pressure and relative permeability drainage curves with various fluid pairs. *Water Resources Research*, :in preparation, 2013.

[115] Leas, WJ , JH Jenks, and C. Russell. Relative permeability to gas. *Journal of Petroleum Technology*, 2(3):65–72, 1950.

[116] Ramakrishnan, T.S., and A. Cappiello. A new technique to measure static and dynamic properties of a partially saturated porous medium. *Chemical Engineering Science*, 46(4):1157–1163, 1991.

[117] Bachu, S. Drainage and imbibition CO_2/brine relative permeability curves at in situ conditions for sandstone formations in western Canada *Energy Procedia*, In Press, 2012

[118] Bennion, D.B., and S. Bachu. Drainage and imbibition relative permeability relationships for supercritical CO_2/brine and H_2S/brine systems in intergranular sandstone, carbonate, shale, and anhydrite rocks. *SPE Reservoir Evaluation and Engineering*, June:487–496, 2008.

[119] Bennion, D.B., and S. Bachu. Drainage and imbibition CO_2/brine relative permeability curves at reservoir conditions for carbonate formations. In *SPE Annual Technical Conference and Exhibition*, SPE 134028, 2010.

[120] Berg, S., S. Oedai, and H. Ott. Displacement and mass transfer between saturated and unsaturated CO_2-brine systems in sandstone. *International Journal of Greenhouse Gas Control*, In Press, 2011.

[121] Perrin, J-C., and S. Benson. An experimental study on the influence of sub-core scale heterogeneities on CO_2 distribution in reservoir rocks. *Transport in Porous Media*, 82(1):93–109, 2009.

[122] W. Yan, G.-Y. Zhao, G.-J. Chen, and T.-M. Guo. Interfacial tension of (methane + nitrogen) + water and (carbon dioxide + nitrogen) + water systems. *Journal of Chemical and Engineering Data*, 46(6):1544–1548, 2001.

[123] Chun, B-S., and G. T. Wilkinson. Interfacial tension in high-pressure carbon dioxide mixtures. *Industrial and Engineering Chemistry Research*, 34(12):4371–4377, 1995.

[124] Kestin, J. and I.R. Shankland. Viscosity of aqueous NaCl solutions in the temperature range 25-200°C and in the pressure range 0.1-30 MPaaCl solutions in the temperature range 25-200°c and in the pressure range 0.1-30 MPa. *International Journal of Thermophysics*, 5(3):241–263, 1984.

[125] Müller, N. Supercritical CO_2-brine relative permeability experiments in reservoir rocks—literature review and recommendations. *Transport in Porous Media*, 87(2):367–383, 2011.

[126] Leverett, M.C. Capillary behavior in porous solids. *Petroleum Transactions (AIME)*, 142:152–169, 1941.

[127] Keelan, D.K. and V.J. Pugh. Trapped-gas saturations in carbonate formations. *SPE Journal*, 15(2):149–160, 1975.

[128] Naar,J., R.J. Wygal, and J.H. Henderson. Imbibition relative permeability in unconsolidated porous media. *SPE Journal*, 2(1):13–17, 1962.

[129] Wardlaw, N.C. The effects of pore structure on displacement efficiency in reservoir rocks and in glass micromodels. In *SPE/DOE Enhanced Oil Recovery Symposium, Tulsa, Oklahoma (USA), April 20-23*, 1980.